Analytical solution of the SIR-model for the temporal evolution of epidemics. Part A: time-independent reproduction factor

Author(s):
Kröger, Martin (iD); Schlickeiser, Reinhard

Analytical solution of the SIR-model for the temporal evolution of epidemics. Part A: time-independent reproduction factor

M Kröger[1],[*] and R Schlickeiser[2,3],[*]

[1] Polymer Physics, Department of Materials, ETH Zurich, Zurich CH-8093, Switzerland
[2] Institut für Theoretische Physik, Lehrstuhl IV: Weltraum- und Astrophysik, Ruhr-Universität Bochum, D-44780 Bochum, Germany
[3] Institut für Theoretische Physik und Astrophysik, Christian-Albrechts-Universität zu Kiel, Leibnizstr. 15, D-24118 Kiel, Germany

E-mail: rsch@tp4.rub.de and mk@mat.etz.ch

CrossMark

Abstract

We revisit the susceptible-infectious-recovered/removed (SIR) model which is one of the simplest compartmental models. Many epidemological models are derivatives of this basic form. While an analytic solution to the SIR model is known in parametric form for the case of a time-independent infection rate, we derive an analytic solution for the more general case of a time-dependent infection rate, that is not limited to a certain range of parameter values. Our approach allows us to derive several exact analytic results characterizing all quantities, and moreover explicit, non-parametric, and accurate analytic approximants for the solution of the SIR model for time-independent infection rates. We relate all parameters of the SIR model to a measurable, usually reported quantity, namely the cumulated number of infected population and its first and second derivatives at an initial time $t = 0$, where data is assumed to be available. We address the question of how well the differential rate of infections is captured by the Gauss model (GM). To this end we calculate the peak height, width, and position of the bell-shaped rate analytically. We find that the SIR is captured by the GM within a range of times, which we discuss in detail. We prove that the SIR model exhibits an asymptotic behavior at large times that is different from the logistic model, while the difference between the two models still decreases with increasing reproduction factor. This part A of our work treats the original

SIR model to hold at all times, while this assumption will be relaxed in part B. Relaxing this assumption allows us to formulate initial conditions incompatible with the original SIR model.

Keywords: statistical analysis, epidemic spreading, coronavirus, extrapolation, SIR epidemic model, asymptotic behavior, analytic approximant

(Some figures may appear in colour only in the online journal)

1. Introduction

Several recent studies [1–4] have demonstrated that the normal or Gaussian distribution function for the temporal evolution of the daily number of new cases (deaths, or alternatively infections) at time t due to the COVID-19 pandemic disease provides quantitatively correct descriptions for the monitored rates in many different countries during a single wave. If applied early enough at the beginning of a pandemic wave, within the regime of non-exponential growth, the Gauss model (GM) makes realistic and reliable predictions for the future evolution of the first wave. It has been argued that the assumption of a Gaussian time evolution is well justified by the central limit theorem of statistics [3], an agent-based model [4], a Taylor expansion [4], or as a special case of the SIR (susceptible-infectious-recovered/removed) model [2]. A motivation of the present manuscript was to provide more rigorous arguments in favor of using the GM to estimate the characteristics (peak time, height, and width) of a first epidemic wave well ahead of its climax.

To describe the time evolution of pandemic deceases many models have been developed which are based on the original deterministic compartmental SIR-model pioneered by Mc-Kendrick and Kermack [5] and its later variants such as the SEIR-model (for recent review see Estrada [6]). Important modifications to these mean-field rate equations include stochastic aspects to account properly both, for strong number fluctuations, driving the continuous phase transition of the system near the epidemic threshold, and also for spatially correlated clusters and spreading fronts caused by the disease transmission through nearest-contact infection [7, 8]. It is hoped that with these important modifications the so improved SIR models ultimately provide quantitatively correct descriptions for the forecast of pandemics in many countries, even beyond the exponential growth phase of the pandemic. The inclusion of the stochastic effects mentioned above is often done by combining numerical computer simulations with the mean-field rate equations of the SIR- or SEIR-models with constant values of the infection and reaction rates. Therefore these studies will also profit from more general analytical solutions to the SIR-model equations for time-dependent infection and recovery rates which we develop here.

On our way we discovered a new analytical solution of the standard SIR-model [5, 9–13] without vital dynamics describing the temporal evolution of the COVID-19 pandemic disease that applies to the whole range of parameters. This solution allows for an arbitrary time dependence of the infection and recovery rates but assumes that the ratio of the two rates is independent of time. We emphasize that the assumption of a constant value for the ratio k of the recovery to the infection rate is necessary to deduce an analytical solution for the SIR model equations. There is no reason why the ratio of these two rates should be constant, as the recovery rate $\mu(t)$ is largely determined by the nature of the disease which is not expected to change strongly over time, whereas on the other hand, the infection rate $a(t)$ is affected by many factors, not the least mitigation measures introduced by the government. Even if we ignore the latter non-pharmaceutical interventions (NPIs) it is not obvious that the infection

rate varies proportional to the recovery rate. Nevertheless we are convinced that our calculations based on a constant value of the ratio k are meaningful and important, basically for the following four reasons: first, our case generalizes earlier treatments where time-independent infection and recovery rates were adopted. Secondly, as our solution allows for an arbitrary time dependence of the infection and recovery rates, despite their constant ratio, it is possible for the first time to model analytically the influence of mitigation measures on the time evolution of epidemics as done in reference [14]. Thirdly, our analytical solution can serve as a benchmark for the verification of numerical solutions of the SIR-model and their variants. Fourthly, if the intrinsic time scales of the pandemic event and the taken mitigation measures are rapid enough we may use our analytical results derived for a constant value of k to study slowly time-varying ('adiabatic') time-dependences $k(t)$ by inserting these slow time variations into our final analytical expressions for k. Such a Wentzel–Kramers–Brillouin-approximation has proven useful in many branches of propagation and transport theory of physics including quantum mechanics.

Moreover, in contrast to earlier work we will also calculate analytically the daily differential rate of newly infected persons resulting from the SIR-model which is the key quantity to compare with the monitored data in different countries, as the size of the currently infected, and not yet recovered, compartment is usually not known. Its asymptotic behavior, peak time and peak amplitudes will all be obtained analytically and exactly.

Besides providing analytic expressions for the quantities characterizing the solution of the SIR model, we derive a simple, accurate approximant that can be used in practice, and shares all relevant features with the exact solution, as we will show. This is a significant improvement compared with approaches, where the solution of the SIR model was for example expanded into a divergent but asymptotic series [15, 16], or where it had been obtained assuming inequalities that do hold only within a very limited range of SIR parameters, as we will show.

As a side-observation we find that the SIR model exhibits an asymptotic behavior at large times that is qualitatively different from the logistic model, while the difference between the two models still decreases with increasing reproduction factor. Because the SIR model is sometimes used with arbitrary initial conditions, we recall here that initial conditions must be interrelated if the SIR model is assumed to hold at all times. This is the scenario to be investigated here, for reasons to be discussed in detail. The present investigation can be extended to the many variants of the SIR model [17–25].

2. SIR-model

As the dynamics of the COVID-19 pandemic is much faster than the dynamics of births and deaths, the neglect of these demographic factors is well justified. The SIR system is the simplest of the compartmental models used for the mathematical modeling of infectious diseases. The considered population of $N \gg 1$ persons is assigned to the three compartments S (susceptible), I (infectious), or R (recovered/removed). Persons from the population may progress between these compartments.

2.1. Basic equations

In a fixed population of individuals let $S(t)$, $I(t)$ and $R(t)$ denote the susceptible, infected and recovered/removed fractions of persons involved in the infection at time t, so that

$$S(t) + I(t) + R(t) = 1 \tag{1}$$

and because S, I, R are fractions, they must all reside within the interval [0,1]. If $a(t)$ and $\mu(t)$ denote the semipositive time-dependent infection and recovery rates, respectively, the SIR-model is defined with the two dynamical equations [5, 9, 26]

$$\dot{I}(t) = a(t)S(t)I(t) - \mu(t)I(t) \tag{2}$$

$$\dot{S}(t) = -a(t)S(t)I(t). \tag{3}$$

where the dot here and in the following denotes a derivative with respect to t. The equation for the dynamics of $R(t)$ follows from the sum constraint (1), i.e.

$$\dot{R}(t) = -\frac{\mathrm{d}}{\mathrm{d}t}[S(t) + I(t) - 1] = \mu(t)I(t), \tag{4}$$

where we inserted equations (2) and (3). Equation (3) can be written as

$$\frac{\dot{S}(t)}{S(t)} = \frac{\mathrm{d}\ln S(t)}{\mathrm{d}t} = -a(t)I(t), \tag{5}$$

so that

$$I(t) = -\frac{1}{a(t)}\frac{\mathrm{d}\ln S(t)}{\mathrm{d}t}, \tag{6}$$

implying that equation (4) becomes

$$\dot{R}(t) = -k(t)\frac{\mathrm{d}\ln S(t)}{\mathrm{d}t} \tag{7}$$

with the potentially time-dependent inverse reproduction factor

$$k(t) = \frac{\mu(t)}{a(t)} \tag{8}$$

The solution and its analytic approximant to be derived in this work holds for arbitrary $a(t)$, as long as $\mu(t)$ and $a(t)$ remain proportional to each other. In that case k is a constant, usually denoted as inverse basic reproduction number, $k = 1/r_0$.

2.2. Initial conditions: all-time versus semi-time SIR

There are two qualitative very different cases to be considered that can be regarded as equally valid approaches. We refer to these cases as the all-time case (I) and the semi-time case (II).

For the all-time case (I), treated by Kendall [9] and part A of this work, the ratio $k = \mu(t)/a(t)$ is regarded as identically constant at all times, from $t = -\infty$ to $t = \infty$. This implies, that one has to use boundary conditions $S(-\infty) = 1$, $I(-\infty) = 0$, $R(-\infty) = 0$ as the epidemic must not have existed at $t = -\infty$. For the special case of $k = 0$, $\mu(t) = 0$ and $R(t) = 0$ at all times according to equation (7), while equations (1)–(3) reduce to $I(t) = 1 - S(t)$ and the simple logistic differential equation $\dot{S}(t) = -a(t)S(t)[1 - S(t)]$ determining all fractions analytically in terms of $a(t)$ (appendix F).

For constant $k > 0$, equation (7) implies the important relation [9]

$$S(t) = S(t')e^{[R(t')-R(t)]/k} \tag{9}$$

valid for any choice of t and t'. Upon inserting the stated boundary conditions at $t' = -\infty$ into equation (9), $S(t)$ and $R(t)$ are simply related via $S(t) = e^{-R(t)/k}$ or $R(t) = -k \ln S(t)$. A special case of this relationship is

$$S(0) = e^{-R(0)/k} \tag{10}$$

In view of equation (1), there remains the freedom to just specify one single initial condition at a certain $t = 0$, where data may have become available. One may regard the time $t = 0$ when the existence of the pandemic wave in the society is realized and monitoring of newly infected persons starts. Besides k there is thus a second parameter of the SIR model, which we denote by the positive ε as it usually represents a small number, but our results are valid for any ε. We define ε via the susceptible fraction of the population at time $t = 0$,

$$S(0) = e^{-\varepsilon} \tag{11}$$

There is no freedom for the remaining $R(0)$ and $I(0)$ if k is known. Inserting the above boundary conditions into equation (10), and making use of equation (1) one has

$$R(0) = k\varepsilon, \qquad I(0) = f_k(\varepsilon) \tag{12}$$

involving a function in $f_k(\varepsilon)$ that is going to frequently occur in this work

$$f_k(x) = 1 - kx - e^{-x} \tag{13}$$

Here $R(0)$ and $I(0)$ represent the recovered/removed and infected fractions of the population at time $t = 0$. For small $\varepsilon \ll 1$ one can write $I(0) \approx (1 - k)\varepsilon$. In turn, if two initial values are known at $t = 0$, the basic reproduction number is given by the initial conditions. We prefer to treat the inverse basic reproduction number k and ε as variables, so that $R(0)$ and $I(0)$ are determined by this set. Any other choice of two variables from the set $k, \varepsilon, I(0)$, and $R(0)$ would work equally well, as the two remaining ones are then given by equation (12).

It it important to realize that the all-time case (I) has solutions only for a limited range of k values. While there is no recovery when $k = 0$ due to equation (7), for $k > 1$ the number of infected would drop (proven below) rather than grow from the boundary value $I(-\infty) = 0$, which is not possible as $I \in [0, 1]$. For $k = 1$, $I(0) = f_1(\varepsilon) = 1 - \varepsilon - e^{-\varepsilon}$ is negative for any $\varepsilon > 0$, and simply remains at its boundary value $I(-\infty) = I(0)$ for $\varepsilon = 0$, and thus $I(t) = 0$ at all times for $k = 1$. Finally, because $I(0) \geqslant 0$ must hold, not all values in $k \in (0, 1)$ are compatible with the initial condition (11) at time $t = 0$. The requirement $I(0) \geqslant 0$ is equivalent with $k \leqslant k_{\max}$ with

$$k_{\max} = \frac{1 - S(0)}{\varepsilon} = 1 - \frac{\varepsilon}{2} + O(\varepsilon^2) \tag{14}$$

This is why the remaining meaningful range of k values is $k \in (0, k_{\max})$ for case (I). As the SIR model is assumed to hold at all times, its solution allows to calculate all fractions at times before and after $t = 0$. These two features make case (I) qualitatively very different from case (II).

In contrast, for the semi-time case (II) treated by Kermack and McKendrick [5] and in part B of this work, the SIR model is not assumed to hold at all times, but only at times $t \geqslant 0$, the time for which feed data may be available. In that case the model cannot be used to calculate fractions at times prior to $t = 0$, as this would under many circumstances lead to $S > 1$ or $I \notin [0, 1]$ at times prior to the 'observation' time $t = 0$. Because the boundary conditions of case (I) must not be respected anymore in that case, one can use arbitrary initial

conditions incompatible with equation (12). The model in this setup has therefore three inde-
pendent parameters such as k, $S(0)$ and $I(0)$, while the remaining $R(0)$ is given by equation (1).
If one chooses the initial conditions to satisfy equation (12), we are back at case (I). Case (II)
therefore chooses initial conditions incompatible with equation (12) such as $S(0) = 1 - \epsilon$ and
$I(0) = \epsilon$, implying $R(0) = 0$. In that case one has moreover the freedom to choose $k > 1$, as it
does not automatically lead to $I \notin [0, 1]$.

Case (II) is thus more flexible, but cannot be used to adequately describe the past. While case
(I) can be considered as the solution to the SIR model over the whole time domain, case (II)
can be used to study the future and the case $k > 1$ of relevance toward the end of an epidemics.
In this work we are going to study case (I) and have to thus assume $k \in (0, 1)$ and $\varepsilon \geqslant 0$.

2.3. Three important remarks

First, as has been noted before [9], in the three dynamical equations (2), (3) and (6) there
is migration from the S-compartment (susceptible) to the I-compartment (infected) at a rate
proportional to SI, and removal from the I-compartment to the R-compartment (recovered,
dead or isolated) at a rate proportional to I; there is no exit from the R-compartment and no
entry into the S-compartment.

Secondly, it is necessary to start initially at time $t = 0$ with at least one infected person,
i.e., $I(0) = f_k(\varepsilon) > 0$ (see the second initial condition (12)), as the dynamical equation (2)
implies for the initial change $\dot{I}(t = 0) = 0$ if $I(t = 0) = 0$. Nothing can grow out of nothing; a
situation very similar to kinetic plasma instabilities where seed electromagnetic fluctuations,
often from spontaneous emission [27], are needed for starting the instability. Keeping exact
tract of the initial conditions during the analysis will prove to be essential to avoid mathematical
singularities in the analysis.

Thirdly, the first term on the right-hand side of the dynamical equation (2) denotes the newly
infected population fraction, i.e., the differential rate of the total fraction $J(t)$ of persons that
have ever been infected, i.e.

$$\dot{J}(t) = a(t)S(t)I(t) = -\dot{S}(t), \tag{15}$$

where the second equality results from equation (3). It is this rate $\dot{J}(t)$ that can be measured, is
usually reported by health agencies along with the cumulative fraction $J(t) = \int_{-\infty}^{t} \dot{J}(\xi)d\xi$, and
that has been modeled by the Gaussian time evolution in our earlier work [3, 4]. Because $S(0)$,
$I(0)$ are usually not reported as they cannot be measured directly, we will show how to replace
SIR parameters k and ε by an initial condition for the typically available $J(0)$ and $\dot{J}(0)$.

3. Results

Throughout this work we use the bar-notation $\widetilde{q}$ if we approximate a quantity q.

3.1. Reduced time

We are here assuming that the infection and recovery rates have the same time dependence, so
that their semipositive ratio is time-independent:

$$\frac{\mu(t)}{a(t)} = \frac{\mu_0}{a_0} = k = \frac{1}{r_0} \in [0, 1) \tag{16}$$

corresponding to a SIR-basic reproduction number $r_0 > 1$. We emphasize that this special
case includes the standard case used by most analysis before that the infection and recovery

rates are constants with respect to time. Equation (16) still allows us to take into account an arbitrary time-dependence of the infection rate $a(t)$ which, of course, then is identical to the time dependence of the recovery rate $\mu(t)$ due to assumption (16). Then it is convenient to introduce for arbitrary time dependence of the infection rate $a(t)$ the new dimensionless time variable τ with $\tau(0) = 0$ via

$$\tau(t) = \int_0^t \mathrm{d}\xi a(\xi), \tag{17}$$

so that

$$\frac{1}{a(t)} \frac{\mathrm{d}}{\mathrm{d}t} = \frac{\mathrm{d}}{\mathrm{d}\tau} \tag{18}$$

Using the reduced time τ, equations (2), (6), and (7) simplify to

$$\frac{\mathrm{d}\ \ln\ I(\tau)}{\mathrm{d}\tau} = S(\tau) - k, \qquad I(\tau) = -\frac{\mathrm{d}\ \ln\ S(\tau)}{\mathrm{d}\tau}, \tag{19}$$

and

$$\frac{\mathrm{d}R(\tau)}{\mathrm{d}\tau} = kI(\tau) = -\frac{\mathrm{d}}{\mathrm{d}\tau}[k\ \ln\ S(\tau)], \tag{20}$$

respectively. In equation (19) $(\mathrm{d}\ln S/\mathrm{d}\tau)_{\tau=0} = -f_k(\varepsilon)$ in order to meet the initial condition (12) for $I(\tau = 0) = f_k(\varepsilon)$.

Equation (19) includes the well-known threshold [5, 9] value k which determines the so-called J-shape or peak-shape [9] of the pandemic wave. Obviously, equation (19) indicates that a peaked pandemic wave cannot emerge if the ratio $k > 1$: as $S \leqslant 1$ the right-hand side of equation (19) in this case is always negative, so that with positive $I(\tau)$ the time derivative $\mathrm{d}I/\mathrm{d}\tau < 0$, so that the infection rate decreases with time. An epidemic wave emerges if the ratio $k < 1$; the case $k = 1$ we already discussed in section 2.2.

The boundary conditions $S(t) = 1$ and $R(t) = 0$ for $t = -\infty$ take over to $S(\tau = -\infty) = 1$ and $R(\tau = -\infty) = 0$ for $k > 0$, because a positive k implies $\mu(t) > 0$ for all t, and thus also $a(t) > 0$ for all t. The solution to equation (20) is thus formally equivalent to the relationship we had between $R(t)$ and $S(t)$,

$$R(\tau) = -k\ \ln\ S(\tau), \qquad S(\tau) = e^{-\frac{R(\tau)}{k}} \tag{21}$$

3.2. Analytical solution

Since the original pioneering work [5] the procedure to obtain analytical solutions is similar in later work [9, 28] and also here: either (1) one expresses two of the interesting variables $S(t)$, $I(t)$ and $R(t)$ in terms of the third one as done in reference [5], or (2) one expresses all three variables in terms of a suitable chosen function as done in reference [28] and here. In both cases one uses equation (1) to calculate the solution. Inserting equations (19) and (21), equation (1) reads

$$S(\tau) - k\ \ln\ S(\tau) - \frac{\mathrm{d}\ \ln\ S(\tau)}{\mathrm{d}\tau} = 1 \tag{22}$$

We emphasize that this equation fulfills the initial conditions (11) for $\tau = 0$. For given rates $a(t)$ and $k = \mu_0/a_0$ the solution of equation (22) yields the temporal evolution of $S(t)$. Equation (22)

can be written as

$$\frac{\mathrm{d} \ln S}{\mathrm{d}\tau} = \frac{1}{S}\frac{\mathrm{d}S}{\mathrm{d}\tau} = S - k \ln S - 1 \tag{23}$$

or

$$\frac{\mathrm{d}S/\mathrm{d}\tau}{S(S - k \ln S - 1)} = 1, \tag{24}$$

which apart from a different notation corresponds to equations (23) and (27) of Harko *et al* [28]. The solution to the dimensional version of equation (24) had been expanded into a series $S(t) = \sum_{n=0}^{\infty} a_n t^n$ by Barlow and Weinstein [15], who realized that the convergence radius is rather low and suggested to look for solutions with correct asymptotic behavior, as we will do here.

To this end we follow a slightly different but equivalent approach starting out from equation (22). We introduce the quantity $G(\tau)$ by

$$G(\tau) = -\ln S(\tau), \qquad S(\tau) = e^{-G(\tau)} \tag{25}$$

with the initial condition $G(\tau = 0) = \varepsilon$. According to equations (19) and (21) the function G (25) determines

$$R(\tau) = kG(\tau), \qquad I(\tau) = \frac{\mathrm{d}G}{\mathrm{d}\tau} \tag{26}$$

The dynamical equation (22) in terms of $G(\tau)$ reads

$$\frac{\mathrm{d}G(\tau)}{\mathrm{d}\tau} = 1 - kG(\tau) - e^{-G(\tau)} = f_k[G(\tau)] \tag{27}$$

using the function f_k defined in (13). Integrating

$$\frac{\mathrm{d}G/\mathrm{d}\tau}{f_k(G)} = 1 \tag{28}$$

over τ then provides (figure 1)

$$\tau(G) = \int_{\varepsilon}^{G} \frac{\mathrm{d}x}{1 - kx - e^{-x}} \tag{29}$$

where the integration constant was determined from the initial condition $G(\tau = 0) = \varepsilon$. The integrand vanishes at $x = 0$ and at certain $x = G_{\infty}$ to be discussed below. The whole $\tau \in [-\infty, \infty]$ range is thus captured by equation (29) upon varying G between zero and G_{∞}, and vice versa, $G(\tau) \in [0, G_{\infty}]$ determines the range of G.

The solution (29) generalizes the known analytical solutions in the literature [5, 9, 28] as it holds for arbitrary time-dependence of the infection rate $a(t)$. The mentioned known solutions can be reproduced with equation (29) by setting $\tau = a_0 t$ on its left-hand side resulting from a constant injection rate a_0. The parametric solution presented in the original SIR work [5] assumed $G \ll 1$ to simplify the analysis. We will see below that $G_{\infty} \ll 1$ holds only within a very narrow range of k values close to $k = 1$. The contributions within the regime $G \in [0, \varepsilon]$ are usually not considered in numerical schemes while they can be used to verify the proper boundary conditions stated at the very beginning. Harko *et al* [28] did show results for $t > 0$ only, as some of the fractions would get negative or exceed unity at times prior to $t = 0$, using
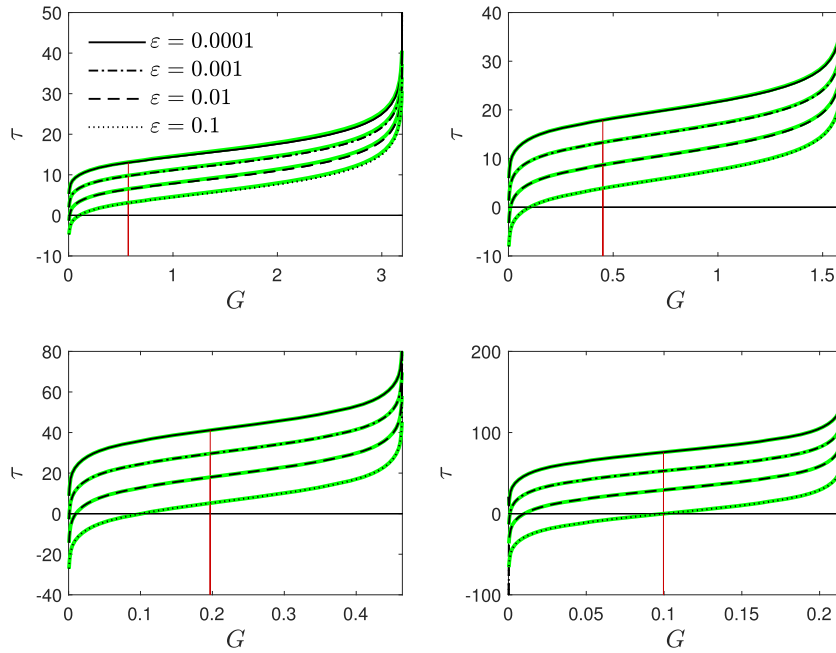
Figure 1. Exact reduced time τ (black) vs G for (a, top left) $k = 0.2$, (b, top right) $k = 0.5$, (c) $k = 0.8$, and (d, bottom right) $k = 0.9$, according to equation (29). Approximant (86) shown in green. The vertical red lines marks $G = G_0$ (54), corresponding to peak time $\tau_0 = \tau(G_0)$. The range of G is given by $G \in [0, G_\infty]$ with G_∞ provided by equation (32) or (34). The relative deviation between exact and approximative versions is plotted in figures 16(a) and (b).

their analytic solution. We will present an equivalent formulation with $\tau(J)$ of the solution (29) in equation (41).

As NPIs during the pandemic wave generate a time-changing infection rate $a(t)$, the generalized solution (29) is highly valuable to assess quantitatively the effect of the NPIs on the time evolution of the disease.

3.3. Maximum value G_∞

The solution (29) indicates that the maximum value $G_\infty = G(\tau = \infty)$ of the function G is attained when the denominator of the integrand vanishes, i.e.

$$f_k(G_\infty) = 0, \tag{30}$$

or

$$e^{-G_\infty} = -k\left(G_\infty - \frac{1}{k}\right) \tag{31}$$

which is of the form (G1) with $c = 1$, $a_0 = -k$ and $r = 1/k$. Consequently, according to equation (G2) we obtain (figure 2)

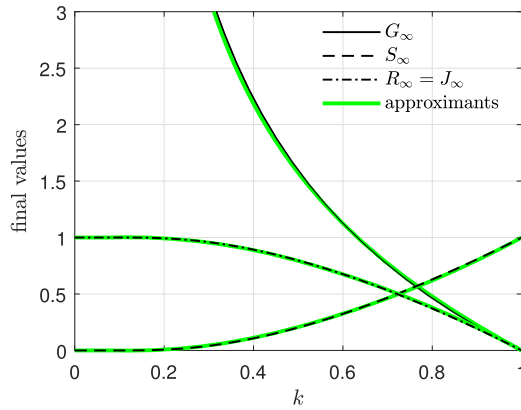$$G_\infty = \frac{1}{k} + W_0(\alpha), \tag{32}$$

Figure 2. Analytic final values G_∞, S_∞, R_∞, and J_∞ vs k (black) according to equations (32), (48), and (49), while $I_\infty = 0$ (48). They are all insensitive to the initial conditions. For all these final values, simple approximants (green) based on equation (34) are shown as well. The relative deviation between exact and approximative versions is plotted in figure 16(c).

where W_0 is the principal solution of Lambert's equation $z = W(z)e^{W(z)}$ (discussed in appendix G) and α is given in terms of k as

$$\alpha = -\frac{e^{-\frac{1}{k}}}{k} \tag{33}$$

The argument α of the Lambert's W_0 function in equation (32) is negative for all k (figure 15(b) in appendix G). Accordingly, $W_0 \in [-1, 0]$ is negative as well (figure 15(a)), while $G_\infty \geqslant 0$. In figure 2 we show the maximum G_∞ as a function of k. It can be seen that G_∞ has values significantly greater than unity for $k \ll 1$, while it vanishes at $k = 1$. The value $G_\infty = 1$ is attained at $k = 1 - 1/e \approx 0.63$. The dashed black line shows the asymptotic behavior of $G_\infty \sim 1/k$ at small $k \ll 1$. Significant deviations from the asymptotic behavior set in at $k \approx 1/3$. According to these considerations, G_∞ is well approximated by (figure 2)

$$\widetilde{G}_\infty \simeq \frac{1}{k} - \frac{8k - 1}{7} \tag{34}$$

The relative error of this approximant is below 2.2% for $k \leqslant 0.63$; its absolute error is below 0.014 for $k \geqslant 0.63$, while it is exact at $k = 1$ and exhibits the correct asymptotic behavior for $k \to 0$.

Similarly, the non-principal solution of Lambert's equation sets the lower bound $G_{-\infty} = G(\tau = -\infty)$ with $G_{-\infty} = k^{-1} + W_{-1}(\alpha) = 0$. The lower bound is identical zero because Lambert's equations is trivially solved by $W_{-1} = -1/k$ for α given by (33). To summarize, $G \in [0, G_\infty]$, compatible with $\tau \in [-\infty, \infty]$ and $S \in [0, 1]$. This compatibility is established as a result of the proper boundary conditions.

3.4. Differential and cumulative rates of newly infected persons

From the invariant $\dot{J}(t)dt = j(\tau)d\tau$ we obtain with equations (25), (27), and equation (17) in the form $d\tau/dt = a(t)$ for differential rate of newly infected persons (figure 3)
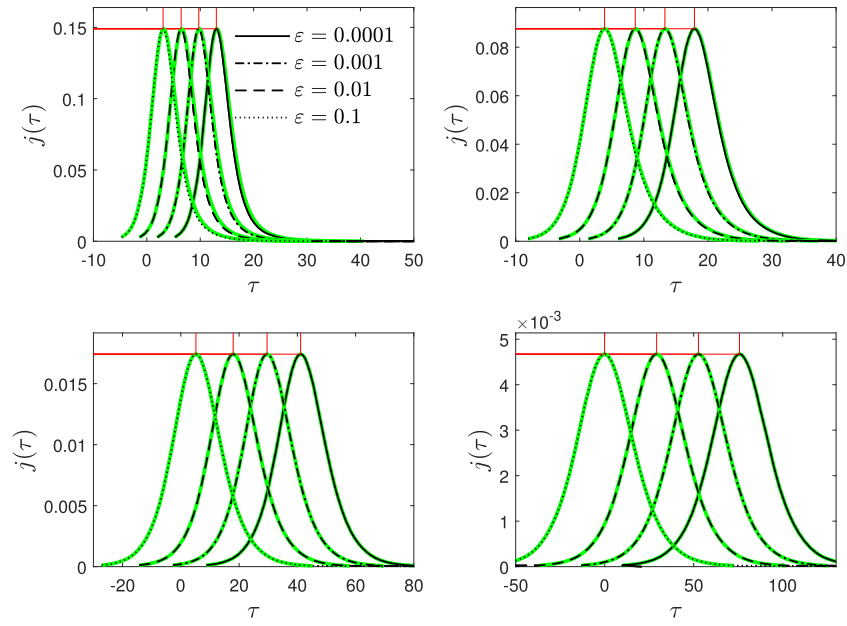
Figure 3. Differential fraction of infected persons $j(\tau)$ (black) vs reduced time τ for (a, top left) $k = 0.2$, (b, top right) $k = 0.5$, (c) $k = 0.8$, and (d, bottom right) $k = 0.9$, according to equation (36). The simple approximant for $j(\tau)$, equations (36) and (86), is shown in green. The peak position, located at τ_0 and $j_{\max}$, is highlighted by vertical and horizontal red lines according to equations (59) and (58). The initial value at $\tau = 0$ is $j(0) = f_k(\varepsilon)e^{-\varepsilon}$, thus different for each k and ε.

$$j(\tau) = \frac{\dot{J}(t)}{a(t)} = S(\tau)I(\tau) = -\frac{dS(\tau)}{d\tau} \tag{35}$$

$$= f_k(G(\tau))e^{-G(\tau)} \tag{36}$$

with the initial value $j(\tau = 0) = f_k(\varepsilon)e^{-\varepsilon}$. The corresponding cumulative distribution picks up all the newly infected individuals, not only the ones that are going to occur at $t > 0$, i.e., one has (figure 4)

$$J(\tau) = \int_{-\infty}^{\tau} d\tau'\, j(\tau') = -\int_{-\infty}^{\tau} d\tau' \frac{dS(\tau')}{d\tau'} = 1 - S(\tau) = 1 - e^{-G(\tau)} \tag{37}$$

In the far past, both quantities j and J emanated from zero, because $G_{-\infty} = 0$. As indicated we may regard these j and J as functions of $G(\tau)$.

Equation (19) in the form $dS/d\tau = -IS$, and $dI/d\tau = SI - kI$ imply with $j = SI$ from equation (35)

$$\frac{d\,\ln\,j}{d\tau} = S - I - k \tag{38}$$

A maximum of $\ln j$ and j thus occurs when $S - I = k$, while (25) and (28) can be used to write $S - I$ in terms of G
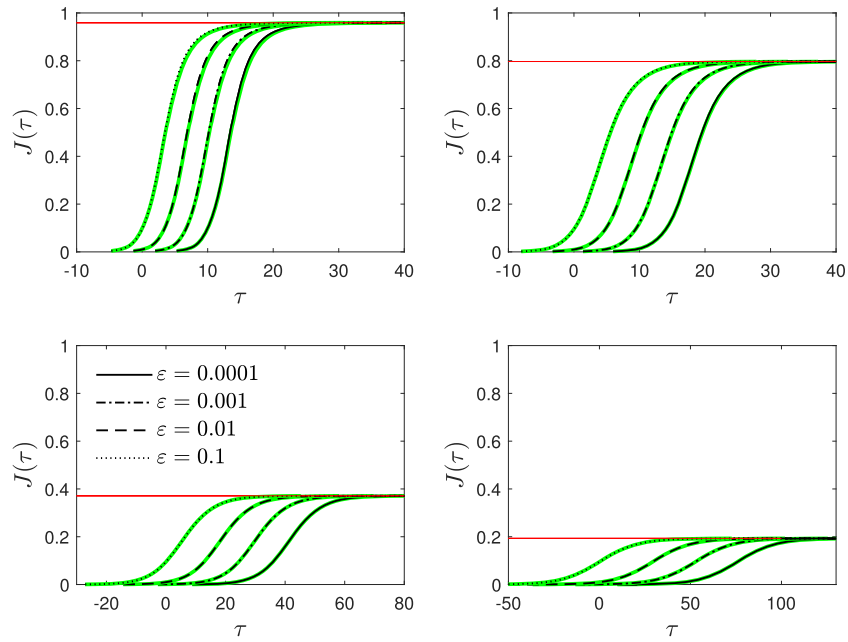
Figure 4. Cumulative fraction of infected persons $J(\tau)$ (black) vs reduced time τ for (a, top-left) $k = 0.2$, (b, top right) $k = 0.5$, (c) $k = 0.8$, and (d) $k = 0.9$, according to equation (37). Approximants (86) shown in green. The final value is $J_\infty = R_\infty = kG_\infty$ (red) with G_∞ from equation (34). Its approximant is given by equation (50).

$$S - I = 2e^{-G} + kG - 1 \tag{39}$$

Hence equation (38) can be written as

$$\frac{\mathrm{d}\ \ln\ j}{\mathrm{d}\tau} = 2e^{-G} + kG - 1 - k \tag{40}$$

Having introduced j and $J = 1 - e^{-G}$, it is worth mentioning that the solution (29) can also be expressed in terms of J as follows. Since $\mathrm{d}G/\mathrm{d}J = (1 - J)^{-1}$,

$$\tau(J) = \int_{J(\varepsilon)}^{J} \frac{\mathrm{d}y}{(1 - y)[y + k\ \ln(1 - y)]} \tag{41}$$

with $J(\varepsilon) = 1 - e^{-\varepsilon}$. The range of J values follows from the range of G values, and is thus given by $J \in [0, J_\infty] = [0, 1 - e^{-G_\infty}] = [0, kG_\infty]$, in light of equation (31). With $\tau(J)$ at hand, the remaining quantities of the SIR model are obtained immediately via $S = 1 - J$, $R = -k\ln(1 - J)$, $I = J - R$, and $j = SI$,

3.5. SIR parameters

The J thus captures all infections up to τ, including those that occurred prior $\tau = 0$, and the usually reported $J(0) = 1 - S(0) = 1 - e^{-\varepsilon}$ provides us with $S(0)$ and ε, i.e.,

$$\varepsilon = -\ln[1 - J(0)] \tag{42}$$

This possibility to determine a parameter does not exist for case (II) where such quantity J is not available from the model equations and can only be manually entered as a new parameter. Only for case (I) it is directly related to $S(\tau)$, as we have just shown. Having determined ε from $J(0)$, and assuming $\tau = a_0 t$ with a constant $a_0 = a(t = 0)$, there are two remaining parameters a_0 and k of the SIR model, that we now obtain from the measurable $J(0)$ and its derivatives $\dot{J}(0)$ and $\ddot{J}(0)$ at the initial $t = 0$. To this end we write down expressions for $\dot{J}(0)$ and $\ddot{J}(0)$ and solve them for k and a_0. The first relationship is obtained from $\dot{J}(t) = a_0 j(\tau)$ given by equation (36), evaluated at $t = 0$. This yields with $f_k(\varepsilon) = 1 - k\varepsilon - e^{-\varepsilon}$ that

$$k = \frac{1 - e^{-\varepsilon} - \dot{J}(0)e^{\varepsilon}/a_0}{\varepsilon} \tag{43}$$

The second relationship follows from $\ddot{J}(0) = a_0 (dj/d\tau)|_{\tau=0}$, using equations (27) and (36). As $dj/d\tau = (dj/dG)f_k(G)$ we can proceed and express $\ddot{J}(0)$ in terms of $G(0) = \varepsilon$, k, and a_0,

$$\ddot{J}(0) = a_0 f_k(\varepsilon)[e^{-\varepsilon} - k - f_k(\varepsilon)]e^{-\varepsilon} \simeq \varepsilon(1 - k)^2 a_0 \tag{44}$$

where the 2nd line can be used if $\varepsilon \ll 1$. Under such conditions

$$\widetilde{a}_0 \simeq \frac{\ddot{J}(0)}{\varepsilon(1 - k)^2} \tag{45}$$

Upon replacing k from equation (43) in equation (45) one can write down an explicit, but lengthy, expression for a_0 in terms of $J(0)$, $\dot{J}(0)$ and $\ddot{J}(0)$. We have thus shown how to obtain all three SIR parameters from the cumulative fraction of newly infected persons J and its derivatives at $t = 0$. In other words, the parameters are obtained from a quadratic fit to the reported $J(t)$, taking into account only data in the vicinity of $t = 0$. Depending on the available data, other expressions presented in this work may be preferred to extract the coefficients, such as equation (68).

3.6. Final values

The knowledge of G_∞ from equation (32) and the solution (29) allow us already to derive a number of important results. We first consider the final values at $\tau = \infty$ of (figure 2)

$$
\begin{aligned}
S_\infty &= S(\tau = \infty) = e^{-G_\infty} = 1 - kG_\infty, \\
I_\infty &= I(\tau = \infty) = \frac{dG_\infty}{d\tau} e^{-G_\infty} = 0, \\
R_\infty &= R(\tau = \infty) = k \, \ln\left[e^{G_\infty}\right] = kG_\infty,
\end{aligned}
\tag{46}
$$

where we have used equations (19), (21) and (25). As a consistency check we note that equation (1) is fulfilled here, i.e. $S_\infty + R_\infty + I_\infty = 1$. Inserting G_∞ from equation (32) we obtain with the help of equation (32)

$$R_\infty = 1 + kW_0(\alpha) = kG_\infty \tag{47}$$

$$S_\infty = 1 - R_\infty(k) = -kW_0(\alpha), \tag{48}$$

which both are determined solely by the inverse basic reproduction number $k = 1/r_0$. In figure 2 we plot the fractions R_∞ and S_∞ from equation (48) as a function of $r_0 > 1$ along with their approximants that follow immediately follow from equations (34) and (46).

If the final values were known, one can calculate the corresponding r_0 upon inverting the relationship between S_∞ and r_0. The result is $r_0 = \ln(S_\infty)/(S_\infty - 1)$. The canonical values $R_\infty = 2/3$ and $S_\infty = 1/3$ are thus reached for $r_0 = 3\ln(3)/2 \approx 1.65$. The final susceptible fraction S_∞ decreases with increasing r_0, starting with $S_\infty = 1$ at $r_0 = 1$, and reaching $S_\infty = 0$ as r_0 grows.

For these values of the differential and cumulative rates of newly infected persons after infinite time we obtain with equations (35) and (46)

$$
\begin{aligned}
j_\infty &= j(\tau = \infty) = I_\infty S_\infty = 0, \\
J_\infty &= J(\tau = \infty) = 1 - S_\infty = R_\infty = kG_\infty
\end{aligned}
\tag{49}
$$

J_∞ thus coincides with R_∞ (figure 2). Its approximant based on equation (34) is

$$
\widetilde{J}_\infty \approx 1 + \frac{k(1 - 8k)}{7}
\tag{50}
$$

With increasing values of k the cumulative fraction of infected persons decreases from 1 at $k = 0$ to 0 at $k = 1$.

3.7. Bell-shaped differential rate. GM-like solution of the SIR

Equation (36) can also be used, even without the explicit inversion of equation (29), to derive generally valid expressions for the time τ_0 of maximum, the maximum level j_{max} and the dimensionless width ω of the differential rate j, which correspond to the three important parameters characterizing a Gaussian differential rate,

$$
j(\tau) = j_{max} \, e^{-\frac{(\tau - \tau_0)^2}{\omega^2}}
\tag{51}
$$

although here the width ω may not be a τ-independent constant. Assuming a constant ω, equation (51) is known as the GM for the time evolution of the daily number of new infections (or also deaths) [4].

3.7.1. Exact peak amplitude. The maximum of the differential rate (36) occurs when the derivative $dj/d\tau$ in equation (40) vanishes providing

$$
2e^{-G_0} + kG_0 = 1 + k
\tag{52}
$$

directly from equations (38) and (39). Writing this as

$$
e^{-G_0} = -\frac{k}{2}\left(G_0 - \frac{1 + k}{k}\right)
\tag{53}
$$

makes the equation of the form (G1) with $c = 1$, $a_0 = -k/2$ and $r = (1 + k)/k$. The analytic solution of equation (52) is the non-principal solution W_{-1} of Lambert's equation,

$$
G_0 = \frac{1 + k}{k} + W_{-1}(\alpha_0), \qquad \alpha_0 = \frac{2\alpha}{e}
\tag{54}
$$

with α from (33). If W in (54) were the principal solution W_0 of Lambert's equation, with the property $W_0(\alpha) \in [-1, 0]$ and $W_0(\alpha_0) \in [-0.406, 0]$ for $k \in [0, 1]$ (appendix G), then $G_0 = G_\infty + 1 + W_0(\alpha_0) - W_0(\alpha)$ would exceed G_∞. The W in (54) is therefore the

non-principal solution W_{-1} of Lambert's equation with the property $W_{-1}(\alpha_0) \leqslant -2$ for all $k \in [0, 1]$, as shown in appendix G. A simple approximant for G_0 is

$$\widetilde{G}_0 \simeq (1 - k) \left(1 + \frac{5}{9}k \right) \ln 2 \tag{55}$$

It is exact at $k = 0$ and $k = 1$ and has a maximum absolute error of 0.008.

Inserting equation (52) in equation (36) yields an analytic expression for the maximum value

$$j_{\text{max}} = j(G_0) = \left(e^{-G_0} - k \right) e^{-G_0} \tag{56}$$

$$= \frac{k^2}{4} \left\{ [1 + W_{-1}(\alpha_0)]^2 - 1 \right\} \tag{57}$$

$$= \frac{(1 - kG_0)^2 - k^2}{4} \tag{58}$$

where the 1st, 2nd, and 3rd line are obtained with the help of (36), (54), (53), respectively. Since $W_{-1}(\alpha_0) \leqslant -2$ for all $k \in [0, 1]$, the j_{max} is positive. For $k = 1$ the $W_{-1}(\alpha_0) = -2$ and j_{max} vanishes. For $k \to 0$ the $W_{-1}(\alpha_0)$ diverges to $-\infty$ (appendix G), but the k^2 in front causes j_{max} to approach $1/4$. Note that j_{max} (58) is not affected by ε but is solely determined by the inverse basic reproduction number k. This is reflected by the results shown in figure 3: regardless of ε the maximum value j_{max} remains unchanged for given k. A simple approximant for j_{max} is provided by equation (77).

We recall that the maximum j_{max} in the measurable daily number of new infections is completely different from the maximum population fraction I_{max} of the infected compartment. Because $I(\tau) = f_k(G)$ it achieves its maximum at $I_{\text{max}} = 1 - k + k \ln k$ according to equation (A2).

3.7.2. Peak time. The time, at which j_{max} is reached, need not be positive. The maximum may have occurred already, depending on the initial condition and the value for the inverse basic reproduction number k. According to solution (29) the value of $G_0(k)$ corresponds to the time of maximum $\tau_0(k)$ where G_0 and τ are given by equations (54) and (29). An explicit expression for τ_0 in terms of k and ε is given upon inserting G_0 from equation (54) into equation (86). This yields (figure 5)

$$\tau_0 = \tau(G_0) = \frac{A(\varepsilon) - A(G_0)}{\kappa(1 - k)} \tag{59}$$

with the very useful abbreviations

$$A(x) = \ln \left(1 - \frac{x}{G_\infty} \right) + \ln \left(\frac{G_\infty}{x} \right)^\kappa \tag{60}$$

and (figure 6(a))

$$\kappa = \frac{k[1 + W_0(\alpha)]}{1 - k} \tag{61}$$

where $1 + W_0(\alpha)$ is identical to the crossover x^* from equation (A11). We can use this κ with the feature $\kappa \in (0, 1)$ to rewrite the exact expression (32) as

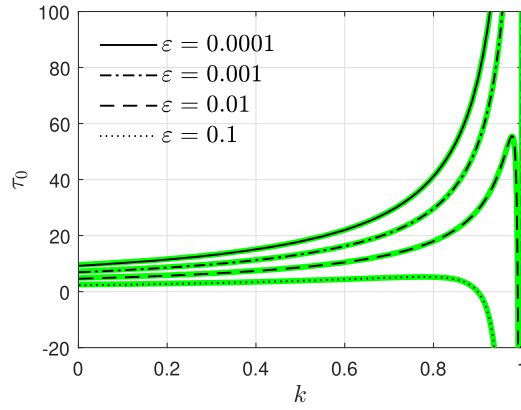$$G_\infty = \frac{(1 - k)(1 + \kappa)}{k} \tag{62}$$

Figure 5. Dimensionless peak time of daily infections, τ_0 vs k for various ε. Exact solution (solid black) compared with the analytic approximant τ_0 (green) from equation (59). The peak time in real units is τ_0/a_0, and corresponds to the number of days between the time of maximum daily infections and the time for which initial conditions have been specified. Because $G_0(k=1) = 0$, depending on the initial condition characterized by ε, the τ_0 becomes negative for sufficiently large k (the peak time has already passed). The relative deviation between exact and approximative versions is plotted in figure 16(d).
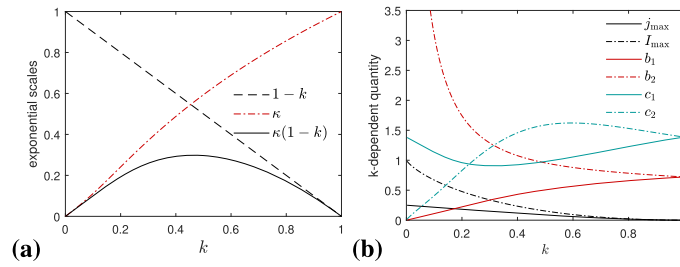

Figure 6. (a) Quantities $1 - k$, κ defined by equation (61) as well as $\kappa(1 - k)$, where $1 - k$ and $\kappa(1 - k)$ characterize the exponential increase and decay of the differential rate j at early and late times. By determining k from the regime of exponential growth at early times, the exponential decrease at late times is already encoded in $\kappa(1 - k)$. (b) Several k-dependent quantities entering the approximant $\widetilde{G}(\tau)$, such as $b_{1,2}$ and $c_{1,2}$ required in equation (87). Also shown is the exact maximum differential rate of newly infected, $j_{\max}$, and maximum fraction of the infected compartment, $I_{\max}$.

Figure 3 indicates that the peak time τ_0 varies inversely with ε, confirming equation (59).

3.7.3. Exact behavior in the vicinity of the maximum.   With the help of equations (28) and (40) one has

$$\frac{\mathrm{d}^2 \ln j}{\mathrm{d}\tau^2} = f_k(G)\frac{\mathrm{d} \ln j}{\mathrm{d}G} = (k - 2e^{-G})f_k(G) \tag{63}$$
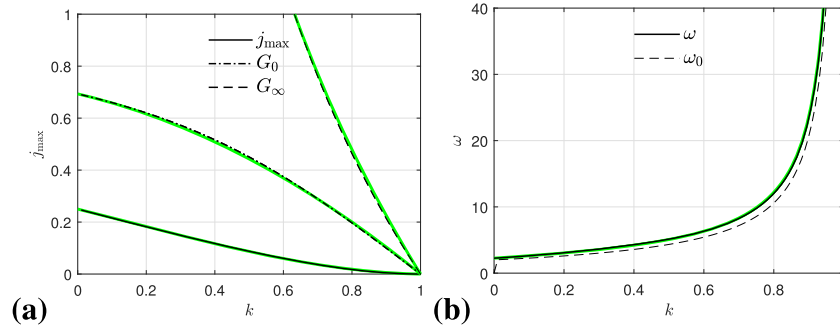
Figure 7. Analytic results (black) for the (a) amplitude j_{max} and (b) widths of the differential rate $j(\tau)$ vs. k according to equations (58), (74) and (66). Also shown in (a): G_0 (54) and G_∞ for comparison with G_0. For all exact results, the simple approximants (34), (55), (76) and (77) are shown for comparison in green.

so that a 2nd order Taylor expansion of $\ln j(\tau)$ around its maximum

$$\ln\ j(\tau) = \ln\ j_{max} + \frac{(\tau - \tau_0)^2}{2} \frac{d^2\ \ln\ j}{d\tau^2}\bigg|_{\tau=\tau_0} + O(\tau - \tau_0)^3 \tag{64}$$

can be evaluated, where $\ln j_{max}$ is given by equation (58). Making use of e^{-G_0} as given by (53), equation (63) evaluated at $\tau = \tau_0$, or equally, $G = G_0$, simplifies to

$$\frac{d^2\ \ln\ j}{d\tau^2}\bigg|_{\tau=\tau_0} = -\frac{2}{\omega_0^2} \tag{65}$$

with (figure 7(b))

$$\omega_0 = \frac{2}{\sqrt{(1 - kG_0)(1 - kG_0 - k)}} \tag{66}$$

We thus have for the Taylor expansion of $\ln j(\tau)$ around its maximum value at τ_0 to second order, $\ln\ j(\tau) = \ln\ j_T(\tau) + O(\tau - \tau_0)^3$ with

$$\ln\ j_T(\tau) = \ln\ j_{max} - \frac{(\tau - \tau_0)^2}{\omega_0^2} \tag{67}$$

with ω_0 given by equation (66).

3.7.4. Exact asymptotic behavior of the SIR model. Next we show that the rate $j(\tau)$ exhibits exponential behavior at early and late times with respect to the peak time and evaluate the growth coefficients.

Making use of the limiting values $G(\tau = -\infty) = 0$ and $G(\tau = \infty) = G_\infty$ in equation (40) we find the growth coefficients characterizing exponential growth and decrease at early and late times,

$$\lim_{\tau \to -\infty} j(\tau) = j_{early} e^{(1-k)(\tau - \tau_0)}, \tag{68}$$

$$\lim_{\tau \to +\infty} j(\tau) = j_{late} e^{-\kappa(1-k)(\tau - \tau_0)} \tag{69}$$

17

with κ from equation (61) and τ_0 from equation (59). Note that the exponent in (68) is positive, and the exponent in (69) is negative since $\kappa > 0$ for all $k \in (0, 1)$.

To calculate the important prefactors in these expressions we start from equation (B2). At small times, where $g = G/G_\infty$ approaches zero, we use the Taylor expansion $\ln(1 - g) = -g$ to obtain

$$G(\tau) \simeq \kappa G_0 W_0 \left[\frac{e^{(1-k)\tau + A(\varepsilon)/\kappa}}{\kappa} \right] \tag{70}$$

for $g \ll 1$ as the solution of equation (B2). Since the argument of Lambert's principal solution W_0 gets small in this limit, cf equation (G10), because $j = (1 - k)G + O(G^2)$, and with the help of τ_0 (59) and $A(x)$ (60) we obtain for the regime of early times $\tau \ll \tau_0$

$$j_{\text{early}} = (1 - k)G_\infty e^{-A(G_0)/\kappa} = (1 - k)G_0 \left(1 - \frac{G_0}{G_\infty} \right)^{-1/\kappa} \tag{71}$$

In the opposite limit, where $g = G/G_\infty$ approaches unity, we can use the Taylor expansion $\ln(g) = g - 1 + O(1 - g)^2$ to obtain

$$G(\tau) \simeq G_\infty \left\{ 1 - W_0 \left[\frac{e^{-\kappa(1-k)} e^{A(\varepsilon)}}{\kappa} \right] \right\} \tag{72}$$

for $1 - g \ll 1$ as the solution of equation (B2). Since the argument of Lambert's function W gets again small in this limit, because $j = \kappa(1 - k)(G - G_\infty)e^{-G_\infty} + O[(G_\infty - G)^2]$, we obtain for the regime at late times $\tau \gg \tau_0$

$$j_{\text{late}} = \kappa(1 - k)G_\infty e^{-G_\infty} e^{A(G_0)} = \kappa(1 - k)(G_\infty - G_0)\left(\frac{G_\infty}{G_0} \right)^\kappa e^{-G_\infty} \tag{73}$$

We have thus shown that the initial condition $S(0)$ enters only the peak time τ_0 and that the prefactors j_{early} and j_{late} characterizing the amplitudes of the asymptotic behaviors depend on k alone. Their dependence on k is shown in figure 8. While j_{early} reaches its maximum at $k \to 0$, where the SIR reproduces the SI model (section 3.6), j_{late} becomes very small in this limit. As a matter of fact, the asymptotic behavior of the SI model, corresponding to a value unity in figure 8, is all that can be observed up to huge times $\tau \sim k^{-1}$ (denoted as τ_c in appendix F), as not only the prefactor j_{late} becomes extremely small in the limit $k \to 0$, but also the contribution $j_{\text{late}}/\kappa(1 - k)$ from the asymptotic exponential to the cumulative J.

These expressions (68), (69), (71) and (73) exactly capture the short and long time behavior of $j(\tau)$ shown in figure 3. The coefficients ε and k can thus also be read off from the regime of exponential growth, if a_0 is already known. It is worthwhile noticing that the initial condition $S(0)$ does only affect the peak time, but not the prefactors j_{early} and j_{late} in the asymptotic behavior of j (figure 9).

3.7.5. Gaussian width. While j is not a perfect Gaussian, as it is not perfectly symmetric (to be discussed below), we can calculate a width via three routes. Route (A) fits $j(\tau)$ by the Gaussian function (51) with constant w. Route (B) determines w by the known GM relationship $w = J_\infty/\sqrt{\pi} j_{\text{max}}$ using our above results for J_∞ and j_{max}. The third route is to estimate a width from the behavior in the vicinity of the peak times. The latter leads to width ω_0 (66). The former two routes give rise to very compatible widths ω as a function of k (all widths shown in figure 7(b)).
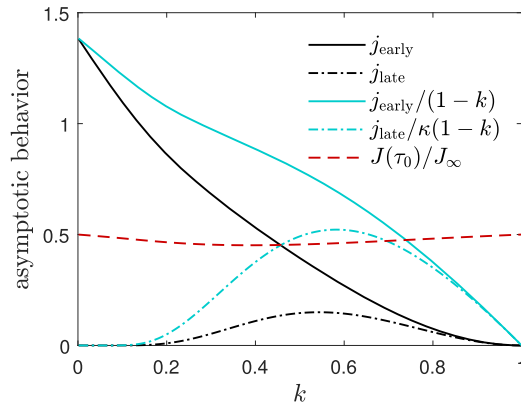
Figure 8. Quantities j_{early} (71) and j_{late} (73) versus k characterize the magnitude of the asymptotic exponential increase and decay of the differential rate j. Also shown are the hypothetical contributions to the cumulative J if j were fully captured by its asymptotes, evaluated at early and late times. The actual contribution from times prior to the peak time τ_0 to the cumulative J is $J(\tau_0)/J_\infty = (1 - e^{-G_0})/kG_\infty$ (shown as well). For the symmetric GM and the logistic model this fraction is $1/2$.
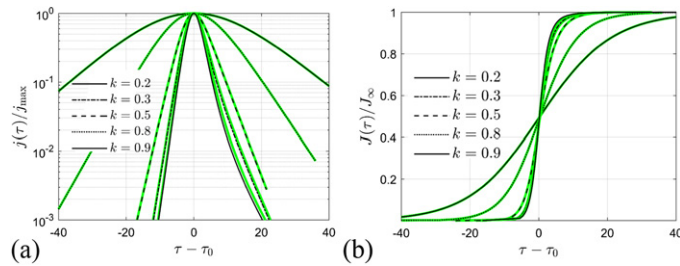

Figure 9. SIR model (a) reduced differential $j(\tau)/j_{\text{max}}$ and (b) reduced cumulative fraction $J(\tau)/J_\infty$ of infected persons versus time relative to peak time, $\tau - \tau_0$, according to equations (36) and (37), with τ_0 from (59), for various k. Approximant (86) shown in green. The asymptotic behaviors of the differential j at small and large τ are in full agreement with our analytic expressions (68) and (69) with (71) and (73).

Making use of our above results (49), (46) and (32), we can thus express a τ-independent characteristic width of $j(\tau)$ analytically as

$$\omega = \frac{4G_\infty}{\sqrt{\pi}k\{[1 + W_{-1}(\alpha_0)]^2 - 1\}} \tag{74}$$

$$= \frac{4G_\infty}{\sqrt{\pi}k[(G_0 - k^{-1})^2 - 1]} \tag{75}$$

where $\alpha_0 = 2\alpha/e$ and α expressed in terms of k in (33), and where we have used G_0 from equation (54). Note, that the width is unaffected by ε as well, it is solely determined by the inverse basic reproduction number k. Taking into account all limiting behaviors our

approximant for ω is given by

$$\widetilde{\omega} \approx \frac{4 + 2k(1-k)}{\sqrt{\pi}(1-k)} \tag{76}$$

implying, with the help of our approximant $\widetilde{G}_\infty$ (34)

$$\widetilde{j}_{\max} = \frac{k\widetilde{G}_\infty}{\sqrt{\pi}\widetilde{\omega}} \approx \frac{(1-k)^2(7+8k)}{14(2-k)(1+k)} \tag{77}$$

Both are compared with the exact results in figure 7. The two frequencies ω_0 and ω are actually very comparable which lead us to the GM-like approximant to be discussed next. We recall that the dimensional $\dot{J}_{\max} = a_0 j_{\max}$ for a constant $a(t)$, and that the dimensional width is then $w = \omega/a_0$.

3.7.6. GM-like approximant for $j(\tau)$. We have by now calculated the behavior of $\ln j(\tau)$ around its maximum including peak height (denoted as $j_T(\tau)$ in equation (67)), and the asymptotic behavior of $j(\tau)$ at small and large τ. Using a continuity requirement we can construct an approximant $\widetilde{j}(\tau)$ for $j(\tau)$ that captures the behavior of $j(\tau)$ qualitatively at all times. The continuity requirement is, in light of equations (68) and (69),

$$\ln\ j_T(\tau_{\text{early}}) = \ln\ j_{\text{early}} + (1-k)(\tau_{\text{early}} - \tau_0), \tag{78}$$

$$\ln\ j_T(\tau_{\text{late}}) = \ln\ j_{\text{late}} - \kappa(1-k)(\tau_{\text{late}} - \tau_0) \tag{79}$$

where j_{early} and j_{late} are given by equations (71), (73), and where the two times τ_{early} and τ_{late} have to be determined by the continuity conditions. The condition (78), with $j_T(\tau)$ from equation (67), yields

$$\tau_{\text{early}} = \tau_0 - \frac{1}{2}(1-k)(1 + D_{\text{early}})\omega_0^2, \tag{80}$$

$$D_{\text{early}} = \sqrt{1 + \frac{4\ \ln(j_{\max}\ /j_{\text{early}})}{(1-k)^2\omega_0^2}} \tag{81}$$

Similarly, condition (79) yields

$$\tau_{\text{late}} = \tau_0 + \frac{1}{2}\kappa(1-k)(1 + D_{\text{late}})\omega_0^2, \tag{82}$$

$$D_{\text{late}} = \sqrt{1 + \frac{4(\ln(j_{\max}\ /j_{\text{late}}))}{\kappa^2(1-k)^2\omega_0^2}} \tag{83}$$

The full GM-like approximant for $j(\tau)$ therefore reads (figure 10)

$$\widetilde{j}_{\text{GML}}(\tau) = \begin{cases} j_{\text{early}}e^{(1-k)(\tau-\tau_0)}, & \tau \leqslant \tau_{\text{early}} \\ j_{\max}\ e^{-(\tau-\tau_0)^2/\omega_0^2}, & \tau \in [\tau_{\text{early}}, \tau_{\text{late}}] \\ j_{\text{late}}e^{-\kappa(1-k)(\tau-\tau_0)}, & \tau \geqslant \tau_{\text{late}} \end{cases} \tag{84}$$

with j_{early} and j_{late} given by equations (71) and (73), κ defined by equation (61), τ_{late} and τ_{late} according to equations (80) and (82), ω_0 specified by equation (66), and τ_0 denoting the peak time $\tau_0 = \tau(G_0)$ from equation (59). The classical GM [4] is a special case of the GM-like approximant for $\tau_{\text{early}} = -\infty$ and $\tau_{\text{late}} \to \infty$.
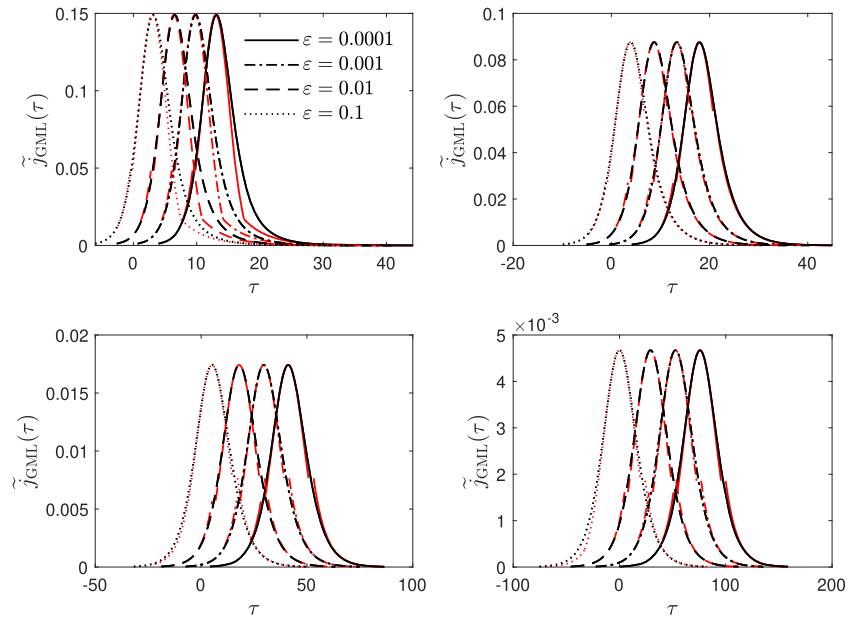
Figure 10. Comparison of the GM-like approximant given by equation (84) (red) and the numerically exact $j(\tau)$ (black) for (a, top left) $k = 0.2$, (b, top right) $k = 0.5$, (c) $k = 0.8$, and (d) $k = 0.9$. The GM-like approximant has three regimes, divided by characteristic times τ_{early} and τ_{late}, where the asymptotic exponential behavior turns into a Gaussian-shaped time-evolution that captures the j in the neighborhood of the peak time. The GM is especially useful prior the climax of the epidemic, where is had been used to estimate the GM parameters. We have shown here how to map these parameters to the parameters of the corresponding SIR model.

Not under all conditions does the central Gaussian part meet the asymptotic exponential tail. Both D_{early} and D_{late} can become complex-valued as soon as the argument of the square root becomes negative. This is the case for D_{late} if τ_0 is sufficiently large and negative. Under such conditions the relevant crossover times are the real parts of τ_{early} and τ_{late}, and the asymptotic branches are only shown up to the level that is reached by $j_T(\tau)$.

Our GM-like approximant (84) suggests that the GM is a suitable approximation for times between τ_{early} and τ_{late}. The ω from equation (74) and ω_0 from equation (66) are found to be very similar, which implies that J_∞ calculated for the GM can serve as an estimate for the exact J_∞, as done in reference [4]. The difference between the GM and the SIR can also be visualized by eliminating time, and plotting j/j_{max} versus J/J_∞ (figure 11).

The value of τ_{early} can be most easily determined from the differential and cumulative doubling times [29] of the GML-approximant (84), as both are constants below t_{early}. t_{early} coincides with the time when the monitored doubling times start to increase with time.

Similarly, τ_{late} can be determined when the differential decay time (although this is seldomly reported) or the cumulative doubling time become constants at late times of a pandemic wave.

The cumulative

$$\widetilde{J}_{\text{GML}}(\tau) = \int_{-\infty}^{\tau} \widetilde{j}_{\text{GML}}(\tau')\mathrm{d}\tau' \tag{85}$$
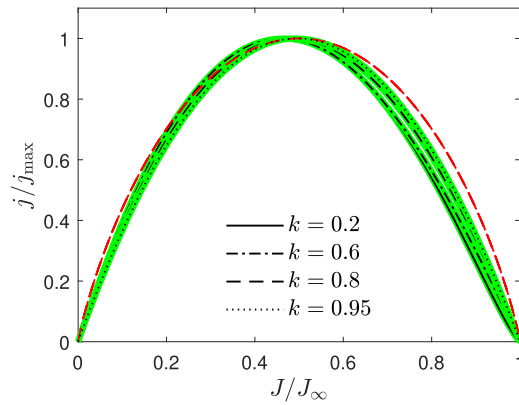
Figure 11. Reduced differential rate $j/j_{\max}$ versus reduced cumulative rate $J/J - \infty$. This representation of the result eliminates time, and thus τ_0. Shown are results of the SIR model for various k (black) together with our approximants $\widetilde{\tau}(G)$ and $\widetilde{G}(\tau)$ (green, both identical in this representation), and the simple GM (red) for comparison. The larger k, the better the simple GM (red) captures the SIR. The GM is especially useful prior the climax of the epidemic, where is had been used to estimate the GM parameters [4].

as well as the final $\widetilde{J}_\infty$ corresponding to the GM-like $\widetilde{j}(\tau)$ then follow by integration. Analytic expressions are provided in appendix H.

4. Further reduction of solution (29)

In order to derive explicit analytical expressions $G(\tau)$ it is necessary to calculate, at least approximately, the remaining integral on the right-hand side of equation (29). Whereas in the references [9, 28] the analytical evaluation of this remaining integral is not detailed, we recall that in the pioneering work [5] this was done for small values of G less than unity by expanding the exponential function in the denominator to second order in x about $x = 0$, i.e. $e^{-x} \simeq 1 - x + x^2/2$. However, this approximation cannot be applied here for all values of G as figure 2 indicates that G_∞ attains values significantly greater than unity. Therefore more generally, without referring to the regime $x \ll 1$, an analytic approximant $\widetilde{\tau}$ for τ can be derived, as shown in appendix A

$$\widetilde{\tau}(G) = \frac{1}{1-k} \left[\ln(G/\varepsilon) + \frac{1}{\kappa} \ln \frac{G_\infty - \varepsilon}{G_\infty - G} \right] \tag{86}$$

that is valid for all $k \in (0, 1)$ and all $\varepsilon \ll 1$. The κ is defined in terms of k by equation (61). We note that equation (86) can alternatively be written as $\widetilde{\tau}(G) = [A(\varepsilon) - A(G)]/\kappa(1-k)$ with A defined by equation (60). Obviously, $\widetilde{\tau}(G = \varepsilon) = 0$ is fulfilled for this approximant. Upon replacing G by G_0 in (86), we arrive at the expression (59) for the peak time. In figure 1 we compared the numerically evaluated integral (29) with the approximation (86) for various k. We notice the excellent agreement.

Even more important in practice, we were able to invert the relationship (86) to obtain an approximant $\widetilde{G}(\tau)$. This is done in appendix (B). There we use this approximant to confirm that it exhibits the correct asymptotic behaviors, that it reproduces the exact $j_{\max}$, and shares the peak time τ_0 with $\widetilde{\tau}(G)$ exactly. To be specific we obtain

$$\frac{\widetilde{G}(\tau)}{G_\infty} = \begin{cases} b_1 W_0[c_1 e^{(1-k)(\tau-\tau_0)}], & \tau \leqslant \tau_0 \\ 1 - b_2 W_0[c_2 e^{-\kappa(1-k)(\tau-\tau_0)}], & \tau \geqslant \tau_0 \end{cases} \tag{87}$$

where the k-dependent parameters $b_{1,2}$ and $c_{1,2}$ (figure 6(b)) are specified in appendix B, τ_0 given by equation (59), and W_0 is the principal solution of Lambert's equation (appendix G). With $\widetilde{G}(\tau)$ at hand, one can express all results in terms of τ, and thus also in terms of time t—for arbitrary $a(t)$—without preparing a parametric plot. The approximant (87) is implemented in appendix J.

5. Time-dependent infection rate *a(t)*

As we have demonstrated, J_∞ and all other final values are insensitive to the precise time-dependency of $a(t)$. It is possible to flatten the curve of daily infections $\dot{J}_{max} = a(t_{max})j_{max}$ by interventions that reduce $a(t_{max})$ at peak time t_{max} given by $\tau_0 = \tau(t_{max})$. Here $\dot{J}_{max}$ is the maximum population fraction that is newly infected within a single day, if we choose day as the time unit in which we also express the infection rate $a(t)$.

While $J(t) = J(\tau)$ is invariant, the differential rates are related as $\dot{J}(t) = \dot{\tau} j(\tau) = a(t)j(\tau(t))$. Inserting $\tau(t)$ for an arbitrarily chosen $a(t)$ into the expression for $j = f_k(G)e^{-G}$ with $G = \widetilde{G}(\tau)$ from equation (87), the daily number of new infections is available analytically as a function of time.

Starting from equations (36) and (37) one has $G = -\ln(1 - J)$ and $S = 1 - J$, so that we can write down a relationship between the differential $j(\tau)$ and the cumulative $J(\tau)$ number of infected persons,

$$j = (1 - J)[J + k \ \ln(1 - J)] \tag{88}$$

The same relationship follows from the derivative of equation (41) with respect to τ. Since $j(\tau) = a(t)\dot{J}(t)$, the infection rate $a(t)$ can be extracted from the measured $\dot{J}(t)$ and $J(t)$ via the right-hand side of equation (88), divided by $\dot{J}(t)$, as long as k is time-independent.

6. Summary and conclusions

We demonstrated that the exact parametric solution $S(t)$, $I(t)$ and $R(t)$ to the SIR model with time-dependent $a(t)$, time-independent k and arbitrary initial conditions is determined by the function $G(\tau)$ uniquely specified equation (29). The t-dependency of G is given by $\tau(t)$ from equation (17). With $G_t = G(\tau(t))$ as a function of t therefore at hand,

$$S(t) = e^{-G_t}, \qquad R(t) = kG_t, \tag{89}$$

and $I(t) = 1 - S(t) - R(t)$ solve the SIR equations at all times, and satisfy the boundary and initial conditions exactly. The measurable differential rate of newly infected $\dot{J}$ and its cumulative counterpart J are then available from $\dot{J}(G_t) = a(t)S(t)I(t)$ and $J(G_t) = 1 - S(t)$, according to equations (36) and (37). Alternatively, one can go over the $J(\tau)$ route instead of $G(\tau)$ as explained in section 3.4.

While the SIR model is usually solved numerically, and the relationship between G and τ given by equation (29) can also be calculated numerically, we provide analytic approximants $\widetilde{G}(\tau)$ (87) as well as for the inverse $\widetilde{\tau}(G)$ (86) that both have the correct asymptotic behaviors and may be use instead of the exact result, as they are sufficiently accurate for any practical purpose. Using this approximant (87), that works for any k and any initial condition, the usually

reported daily number of new infections we have expressed explicitly as a function of time t for an arbitrarily time-dependent infection rate $a(t)$ in section 5. The presented solution of the all-time SIR model can thus be used to replace the numerical solution of the SIR model. Having an analytical solution should be also advantageous to understand the effect of interventions reflected by $a(t)$ much easier, and in a more transparent fashion.

The whole shape of the differential rate j depends on k only. The shape is characterized by the maximum $j_{\max}$ (58), width ω (74), asymptotic exponents $1 - k$ and $-\kappa(1 - k)$ as well as their prefactors j_{early} (71) and j_{late} (73), while the initial condition affects the peak time τ_0 (59). All these quantities have been determined analytically in this work for the all-time SIR model. In addition, we have provided approximants for all quantities characterizing the exact solution of the SIR model, to appreciate their qualitative behavior, or in case the Lambert functions are unavailable. For the special case of time-independent $a(t) = a_0$, and thus $\tau = a_0 t$, the SIR parameters k, ε, and a_0 can all be determined from initial conditions $J(0)$, $\dot{J}(0)$, and $\ddot{J}(0)$ by equations (42), (43) and (45). This is important because the I and R fractions are usually not reported at a certain time to provide an initial condition.

Our derivation not only generalizes existing solutions, but may appear very compact compared with existing ones, while it includes them as a special case. We have relaxed the assumptions of $t \geqslant 0$ and $G \ll 1$ from previous approaches, and present the unique solution that captures consistently both the future and the past, if the SIR model is assumed to hold in the past as well. The classical assumption $G \ll 1$ we have shown to fail except at inverse basic reproduction numbers close to unity.

The evolution of the usually reported differential rates assumes a bell-shaped curve characterized by a peak time τ_0, height $j_{\max}$, and width ω. We have provided analytic expressions for all these parameters by equations (59), (58), and (74), respectively. They involve the two solutions W_0 and W_{-1} of Lambert's equation, usually available in scientific software. To appreciate the validity of our arguments and derivations, we have collected the required exact features of W_0 and W_{-1} in appendix G.

We have inspected the limiting case of $k \to 0$ of the SIR model to find that the SI model, corresponding to $k = 0$, does not trivially emerge from the SIR model in this limit. While the asymptotic behavior of the SIR model is qualitatively different from the SI model, the quantitative difference between them still decreases with decreasing k. Insofar is the SI model compatible with the limiting case of an SIR model, but at the same time asymptotically different.

The semi-time SIR model, which can be considered as the SIR model subject to initial conditions incompatible with the all-time SIR model, and thus useful to predict only the future time-evolution, will be elaborated in part B of this work.

Appendix A. Approximant $\widetilde{\tau}(G)$ for $\tau(G)$

Here we address the formal solution (29)

$$\tau = \int_{\varepsilon}^{G} \frac{\mathrm{d}x}{f_k(x)}, \tag{A1}$$

with f_k defined in (13), over the range of all possible values for $G \in [0, G_\infty]$ and $k \in [0, 1]$, where G_∞ is given by (32). For the special case of $G = G_0$, we thus also address the peak time $\tau_0 = \tau(G_0)$ introduced in section 3.7. The f_k in the denominator of the integral is semipositive, has its maximum at $x_m = -\ln(k)$, and reaches zero at G_∞. A 2nd root of f_k is located at $x = 0$. Accordingly, f_k has the following properties: $f_k(0) = f_k(G_\infty) = 0$, $f'_k(0) = 1 - k$,
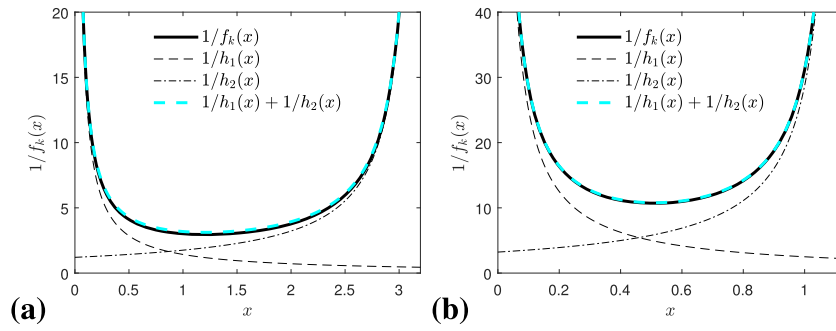
Figure 12. Integrand $1/f_k(x)$ with $f(x)$ defined by (13) for (a) $k = 0.3$ ($G_\infty \approx 3.20$) and (b) $k = 0.6$ ($G_\infty \approx 1.13$) (black). The asymptotic behavior is captured at small x by $1/h_1(x)$ (dashed gray) and at large x by $1/h_2(x)$ (dashed gray). Our approximant (A5) (yellow) appears to basically coincide with the integrand, and has the correct asymptotic behavior by construction.

$f'_k(x_m) = 0$, and

$$f_k^{\max} = f_k(x_m) = 1 - k + k \ \ln \ k, \tag{A2}$$

For $x \ll 1$ the function $f_k(x)$ can be expanded about $x = 0$ as $f_k(x) = h_1(x) + \mathcal{O}(x^2)$ with

$$h_1(x) = (1 - k)x \tag{A3}$$

Likewise, for large x we expand f_k about G_∞ to obtain $f_k(x) = h_2(x) + \mathcal{O}((G_\infty - x)^2)$ with

$$h_2(x) = (x - G_\infty)[1 - k(1 + G_\infty)] = \kappa(1 - k)(G_\infty - x) \tag{A4}$$

with κ from equation (61). Using these asymptotes we obtain the following approximant

$$\frac{1}{f_k(x)} = \frac{1}{h_1(x)} + \frac{1}{h_2(x)} \tag{A5}$$

Examples for the cases of $k = 0.3$ and $k = 0.6$ are shown in figure 12. Both partial integrals can be performed analytically as

$$\tau_1(G) = \int_\varepsilon^G \frac{\mathrm{d}x}{h_1(x)} = \frac{\ln(G/\varepsilon)}{1 - k}, \tag{A6}$$

$$\tau_2(G) = \int_\varepsilon^G \frac{\mathrm{d}x}{h_2(x)} = \frac{1}{\kappa(1 - k)} \ \ln \left[\frac{G_\infty - \varepsilon}{G_\infty - G} \right] \tag{A7}$$

and $\widetilde{\tau}(G) = \tau_1(G) + \tau_2(G)$. While τ_1 dominates the integral at small G, at $G = \varepsilon$ and beyond, τ_2 is responsible for the sharp increase at large G, when G approaches G_∞ (see figure 1). With $A(x)$ defined by equation (60), $\widetilde{\tau}(G)$ can alternatively be written as

$$\widetilde{\tau}(G) = \frac{A(\varepsilon) - A(G)}{\kappa(1 - k)} \tag{A8}$$

The exact asymptotic behaviors at small and large G are

$$\lim_{G \to 0} \tau(G) = \lim_{G \to 0} \tau_1(G) = -\infty, \tag{A9}$$

$$\lim_{G \to G_\infty} \tau(G) = \frac{\ln(G_\infty/\varepsilon)}{1-k} + \lim_{G \to G_\infty} \tau_2(G) = \infty \tag{A10}$$

where the intermediate expressions are also required, e.g., to calculate j_{late} in equation (73).

As already noted, $h_1(x)$ and $h_2(x)$ dominate the behavior of the integrand in distinct x regimes. To specify the regimes, we solve $h_1(x^*) = h_2(x^*)$ to obtain

$$x^* = 1 + W_0(\alpha) = \frac{\kappa(1-k)}{k} \tag{A11}$$

with the help of (32), and where we recall that $W_0(\alpha) \in [-1, 0)$ is negative for all $k \in [0, 1]$. For $x < x^*$ the dominating contribution is $h_1(x)$. While $x^* = 1$ for $k = 0$ and $x^* \approx 1$ for $k < 0.2$, it depends almost linearly on k for larger k and reaches $x^* = 0$ for $k = 1$. From equation (A6) we infer

$$G(\tau) \approx \varepsilon e^{(1-k)\tau}, \qquad G \ll x^* \tag{A12}$$

and G_0 given by equation (54) we can derive from equation (A11) the inequality

$$G_0 \leqslant x^* \tag{A13}$$

for all k, while $G_0 = x^*$ at $k = 1$ follows from the mentioned properties of Lambert's functions.

Appendix B.　Approximant $\widetilde{G}(\tau)$ for $G(\tau)$

Starting from the high quality approximant $\widetilde{\tau}(G)$ derived in the previous section, we are looking for an explicit expression for the inverse function, $\widetilde{G}(\tau)$. Unfortunately, $\widetilde{\tau}(G)$ cannot be inverted analytically over the whole G domain, but we are going to find approximants for G separately over the two disjoint intervals $\widetilde{G} \in [0, G_0]$ and $\widetilde{G} \in [G_0, G_\infty]$ so that

$$\frac{\widetilde{G}(\tau)}{G_\infty} = \begin{cases} g_1(\tau), & \tau \leqslant \tau_0 \\ g_2(\tau), & \tau \geqslant \tau_0 \end{cases} \tag{B1}$$

with g_1, g_2 given in terms of k and ε by equations (B4), (B6) to be derived in this section, and compared with the exact $G(\tau)$ in figure 13. We recall that G_∞ is known in terms of k by equation (32). The two partial approximants meet exactly at $\tau = \tau_0$ specified by equation (59).

To derive all quantities appearing in equation (B1) we start from $\widetilde{\tau} = \tau_1 + \tau_2$ in terms of G, provided by equations (A6) and (A7). Upon introducing $g = G/G_\infty$ and the known $g_0 = G_0/G_\infty$, using the abbreviation κ already introduced by equation (61), the governing equation for g is written

$$\kappa \ln g - \ln(1-g) = \kappa(1-k)\tau - A(\varepsilon) \tag{B2}$$

involving the g-independent and semipositive constant $A(\varepsilon)$ defined by equation (60). Equation (B2) leads to the exact transcendental equation

$$\frac{g^\kappa}{1-g} = e^{\kappa(1-k)\tau - A(\varepsilon)} \tag{B3}$$
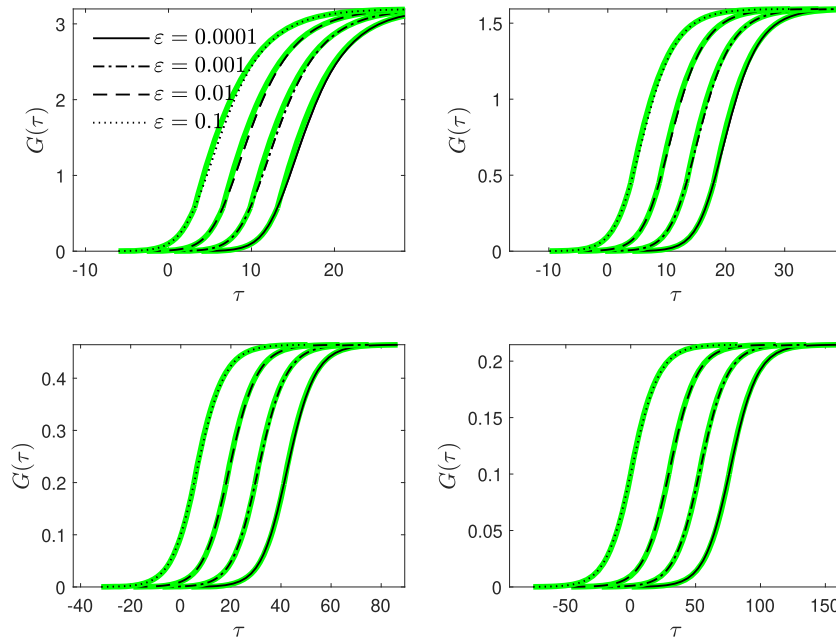
Figure 13. Comparison of the numerically exact $G(\tau)$ (black) with the approximant $\widetilde{G}(\tau)$ from equation (B1) (green) versus τ for various ε and for (a, top left) $k = 0.2$, (b, top right) $k = 0.5$, (c) $k = 0.8$, and (d) $k = 0.9$.

that cannot be solved analytically. To proceed we approximate, for the two cases of $g > g_0$ and $g < g_0$ separately, corresponding to $\tau \leqslant \tau_0$ and $\tau \geqslant \tau_0$, respectively, the smaller of the two logarithmic terms. In each case we make sure that the approximation is correct in all limiting cases, so that not only the asymptotic behavior of G and j will be correctly captured, but also g_1 and g_2 will coincide at $\tau = \tau_0$.

B.1. Approximant $\widetilde{G}_1(\tau) = g_1(\tau)G_\infty$

To obtain g_1 we approximate $\ln(1 - g) \simeq -C_1 g$ in equation (B2) with a constant C_1 in such a way that the approximation is exact at both $g = 0$ and $g = g_0$. This yields $C_1 = -g_0^{-1} \ln(1 - g_0)$. If we furthermore introduce x via $g = e^{-x}$, the corresponding equation for x is of the form (G1) with $c = 1$, $r = A(\varepsilon)/\kappa - (1 - k)\tau$, and $a_0 = \kappa/C_1$. Its solution is thus $x = r + W_0(e^{-r}/a_0)$, involving W_0 and not W_{-1} because the argument $e^{-r}/a_0 \geqslant 0$ (figure 15). With x at hand, we have found $g_1 = \ln x$ which can be written with the help of Lambert's equation in two equivalent ways

$$g_1(\tau) = b_1 W_0(c_1 x_1) = \frac{W_0(c_1 x_1)}{W_0(c_1)} g_0, \tag{B4}$$

both for a different purpose. In equation (B4) we have introduced the abbreviations $b_1 = \kappa/C_1 = -\kappa g_0 / \ln(1 - g_0)$,

$$c_1 = -\frac{\ln(1 - g_0)}{\kappa(1 - g_0)^{1/\kappa}}, \qquad x_1 = e^{(1-k)(\tau - \tau_0)} \tag{B5}$$

with $g_0 = G_0/G_\infty$, so that x_1 carries the dependency on time, and is unity at $\tau = \tau_0$ with τ_0 according to (59), G_0, κ and A explicitly given by equations (54), (61), and (60). This expression for τ_0 is just another way of writing the expression (59) for τ_0 we obtained from $\widetilde{\tau}(G)$ in the previous section. The equivalence follows already from equation (B2). The right-hand side of equation (B4) proves that $g_1(\tau_0) = g_0$.

B.2. Approximant $\widetilde{G}_2(\tau) = g_2(\tau)G_\infty$

For the opposite case of large g close to unity. We use the same strategy as before and now approximate $\ln(g) \simeq C_2(g-1)$ with a constant C_2 in such a way that the approximation is exact at both $g = 1$ and $g = g_0$. This yields $C_2 = -(1-g_0)^{-1} \ln g_0$. If we proceed in a way analogous to the case of g_1, we obtain

$$g_2(\tau) = 1 - b_2 W_0(c_2 x_2) = 1 - \frac{W_0(c_2 x_2)}{W_0(c_2)}(1 - g_0), \tag{B6}$$

Here we have introduced the abbreviations $b_2 = (\kappa C_2)^{-1} = (g_0 - 1)(\kappa \ln g_0)^{-1}$,

$$c_2 = -\frac{\kappa \ln g_0}{g_0^\kappa}, \qquad x_2 = e^{-\kappa(1-k)(\tau-\tau_0)} \tag{B7}$$

so that x_2 carries the dependency on time, is unity at $\tau = \tau_0$, where τ_0 was already given by equation (59).

The two half approximants (B4) and (B6) (figure 13) perfectly match at G_0 by construction, i.e., by the proper choice of the approximants for $\ln(1-y)$ and $\ln y$. The calculations leading to the present form of the approximants had to make use of properties of Lambert's function, in particular the identity $W(z \ln z) = \ln z$ from equation (G6) for any positive z. Note that the dependency of $\widetilde{G}(\tau)$ on ε is adsorbed by x_1 and x_2, while all other coefficients are positive and depend on k only. The coefficients are not independent of each other, as

$$b_2 c_2 = (b_1 c_1)^{-\kappa} = \frac{1 - g_0}{g_0^\kappa} \tag{B8}$$

holds. To summarize, in this section we have provided an explicit expression for the approximant $\widetilde{G}(\tau)$ in terms of k and ε, and also an approximant for the peak time τ_0 in terms of the same parameters. Because the assumptions were asymptotically exact, the approximant has the features

$$\lim_{\tau \to -\infty} \widetilde{G}(\tau) = G_\infty \lim_{x_1 \to 0} g_1(\tau) = \lim_{x_1 \to 0} b_1 c_1 x_1 = 0,$$
$$\lim_{\tau \to \infty} \widetilde{G}(\tau) = \lim_{x_2 \to 0} G_\infty(1 - b_2 c_2 x_2) = G_\infty, \tag{B9}$$

as expected, and $\widetilde{G}(\tau)$ is compared with the exact $G(\tau)$ in figure 13. To arrive at equation (B9), we used property (G10) of the Lambert's function. Approximants $\widetilde{\tau}(G)$ and $\widetilde{G}(\tau)$ are compared with each other in figure 14.

Appendix C. Approximant $\widetilde{S}(\tau)$ for $S(\tau)$

$S(\tau)$ had been defined by equation (25). Using the identity $W(z) = \ln(z) - \ln W(z) = \ln[z/W(z)]$ implies $aW(z) = \ln[z/W(z)]^a$ and $e^{-aW(z)} = [W(z)/z]^a$. We thus have, starting from
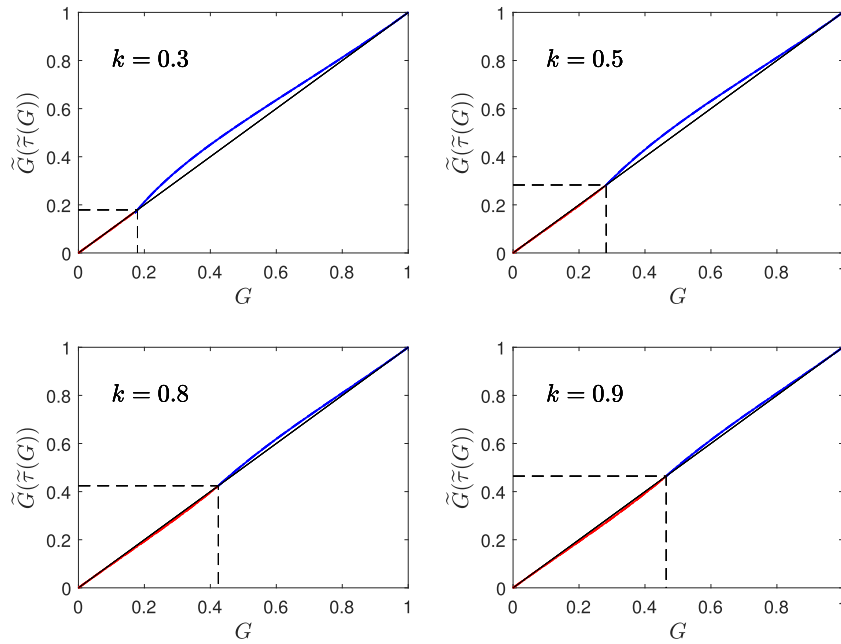
Figure 14. Comparison of the two approximants $\widetilde{\tau}(G)$ and $\widetilde{G}(\tau)$ for (a, top left) $k = 0.2$, (b, top right) $k = 0.5$, (c) $k = 0.8$, and (d) $k = 0.9$. Shown is $\widetilde{G}(\widetilde{\tau}(G))$ versus G, where the part with $G \leqslant G_0$ is colored red, while the remaining part is blue. The dashed lines marks the point (G_0, G_0), and the black line is a guide for the eye. The approximants are inverse to each other independent on the value of ε.

the result of the previous section,

$$\widetilde{S}_1(\tau) = e^{-\widetilde{G}_1(\tau)} \simeq \left[\frac{W_0(c_1 x_1)}{c_1 x_1}\right]^{b_1 G_\infty}, \tag{C1}$$

$$\widetilde{S}_2(\tau) = e^{-\widetilde{G}_2(\tau)} \simeq \left[\frac{W_0(c_2 x_2)}{c_2 x_2}\right]^{-b_2 G_\infty} e^{-G_\infty} \tag{C2}$$

where $\widetilde{S}_1(\tau)$ captures the regime before, and $\widetilde{S}_2(\tau)$ the regime after the peak time τ_0. As these approximants have correct asymptotic behavior, the exact asymptotic behavior of $S(\tau)$ follows from these expressions with equation (G10).

Appendix D. Approximants $\widetilde{I}(\tau)$ and $\widetilde{R}(\tau)$

Since $R = kG$ according to equation (26) and $S + I + R = 1$, we can write immediately down our approximants for $R(\tau)$ and $I(\tau)$

$$\widetilde{R}(\tau) = k\widetilde{G}(\tau), \tag{D1}$$

$$\widetilde{I}(\tau) = 1 - \widetilde{S}(\tau) - k\widetilde{G}(\tau) \tag{D2}$$

$$= 1 - k\widetilde{G}(\tau) - e^{-\widetilde{G}(\tau)} \tag{D3}$$

with $\widetilde{G}$ and $\widetilde{S}$ given by equations (B1) and (C2).

Appendix E. Approximant $\widetilde{j}(\tau)$ for $j(\tau)$

The differential rate $j(\tau)$ had been defined by equation (35) or the equivalent equation (36). With $\widetilde{G}(\tau)$ from equation (B1) at hand we can calculate the approximant for $\widetilde{j}(\tau)$ via equation (36).

$$\widetilde{j}(\tau) = \widetilde{I}(\tau)\widetilde{S}(\tau) \simeq \begin{cases} j_1(\tau), & \tau \leqslant \tau_0 \\ j_2(\tau), & \tau \geqslant \tau_0 \end{cases} \tag{E1}$$

with τ_0 according to equation (59). with the approximants for $\widetilde{I}(\tau)$ and $\widetilde{S}(\tau)$ in terms of $\widetilde{G}$ already written down in equations (D3), (C1), and (C2). Obviously, j_1 meets j_2 at $\tau = \tau_0$, because $G_1(\tau_0) = G_2(\tau_0)$. Note that this is not the case if equation (35) is used, as the slopes of $\widetilde{S}_1$ and $\widetilde{S}_2$ are not exactly identical at $\tau = \tau_0$. The prefactors of this approximant in the asymptotic limits of early and late times differ from the exact equations (71) and (73) only by a factor C_1 and C_2, respectively, introduced in section B. Both factors approach unity for small ε, and start to deviate from unity only at large $\varepsilon \gtrsim 0.2$.

The maximum of the approximant coincides with the exact j_{max}, because we have determined $\widetilde{j}$ using equation (36), and because the definition of G_0 implies $j_{max} = (e^{-G_0} - k)e^{-G_0}$, which remains unchanged, as the maximum of the approximant occurs at $\tau = \tau_0$, where $G = G_0$.

E.1. Remark: non-monotonous $d\widetilde{S}/d\tau$

If we calculate the approximant $\widetilde{j}(\tau)$ starting from equation (35), using the notation from appendix B, with $dx_1/d\tau = (1 - k)x_1$, and the property (G8) of Lambert's function, this gives

$$\widetilde{j}_1(\tau) = -\frac{d\widetilde{S}_1}{d\tau} = -\frac{c_1 dx_1}{d\tau}\frac{dS_1}{d(c_1 x_1)} = \frac{(1-k)G_\infty}{[1 + W_0(c_1 x_1)]}g_1(\tau)\widetilde{S}_1(\tau) \tag{E2}$$

Similarly, with $dx_2/d\tau = -\kappa(1 - k)x_2$,

$$\widetilde{j}_2(\tau) = -\frac{d\widetilde{S}_2}{d\tau} = -\frac{c_2 dx_2}{d\tau}\frac{dS_2}{d(c_2 x_2)} = \frac{\kappa(1-k)G_\infty}{[1 + W_0(c_2 x_2)]}[1 - g_2(\tau)]\widetilde{S}_2(\tau) \tag{E3}$$

At $\tau = \tau_0$, these expressions simplify with $x_1 = x_2 = 1$, $g_1(\tau_0) = g_2(\tau_0) = g_0$, $\widetilde{S}_1(\tau_0) = \widetilde{S}_2(\tau_0)$. We thus have

$$\frac{\widetilde{j}_1(\tau_0)}{\widetilde{j}_2(\tau_0)} = \frac{(1-k)g_0}{[1 + W_0(c_1)]}\frac{[1 + W_0(c_2)]}{\kappa(1-k)(1-g_0)} = \frac{1}{\kappa}\frac{[1 + W_0(c_2)]}{[1 + W_0(c_1)]} \tag{E4}$$

If we now make use of relationships from appendix B, i.e., replace $W_0(c_1) = -\kappa^{-1}\ln(1 - g_0)$, $W_0(c_2) = -\kappa\ln g_0$, and κ by its definition (61), we see that this ratio is unity for a single k, but not all $k \in (0, 1)$. This is because $d\widetilde{S}/d\tau$ is generally non-monotonic.

Appendix F. The case of vanishing *k*

For the extremal case of $k = 0$ (so-called SI model), which is shown here to emerge nontrivially from the SIR model in the limit $k \to 0$, the differential equation (27) for $G(\tau)$ with $G(0) = \varepsilon$ is solved by

$$G_{\mathrm{SI}}(\tau) = \ln(1 + e^{\tau - \tau_0^{\mathrm{SI}}}), \qquad \tau_{\mathrm{SI}}^0 = -\ln(e^\varepsilon - 1) \tag{F1}$$

hence $S_{\mathrm{SI}}(\tau) = e^{-G_{\mathrm{SI}}(\tau)} = 1 - J_{\mathrm{SI}}(\tau) = [1 + e^{\tau - \tau_{\mathrm{SI}}^0}]^{-1}$ and

$$I_{\mathrm{SI}}(\tau) = 1 - S_{\mathrm{SI}}(\tau) = \frac{e^{\tau - \tau_{\mathrm{SI}}^0}}{1 + e^{\tau - \tau_{\mathrm{SI}}^0}} \tag{F2}$$

since $R_{\mathrm{SI}} = 0$ at all times for $k = 0$. The differential rate is given by $G_{\mathrm{SI}}(\tau)$ via equation (36) or via equation (35), or from $\mathrm{d}J_{\mathrm{SI}}/\mathrm{d}\tau$, as

$$j_{\mathrm{SI}}(\tau) = \frac{e^{\tau - \tau_{\mathrm{SI}}^0}}{(1 + e^{\tau - \tau_{\mathrm{SI}}^0})^2} \tag{F3}$$

The same result is obtained with $j_{\mathrm{SI}}(\tau) = I_{\mathrm{SI}}(\tau)S_{\mathrm{SI}}(\tau)$ using the solution of the logistic equation, mentioned in section 2.2. Its maximum with amplitude $j_{\mathrm{SI}}^{\max} = 1/4$ thus occurs at τ_{SI}^0, the asymptotic behavior is given by $\lim_{\tau \to -\infty} j_{\mathrm{SI}}(\tau) = e^{\tau - \tau_{\mathrm{SI}}^0}$ and $\lim_{\tau \to \infty} j_{\mathrm{SI}}(\tau) = e^{-(\tau - \tau_{\mathrm{SI}}^0)}$, and the GM-like behavior in the vicinity of $\tau = \tau_{\mathrm{SI}}^0$ follows from the Taylor-expansion as $j_{\mathrm{SI}}(\tau) \simeq [1 - (\tau - \tau_{\mathrm{SI}}^0)^2]/4$, corresponding to $\omega_0 = 2$. Within the SI model, every person gets infected in the course of time, $J_{\mathrm{SI}}^\infty = 1$, but nobody will ever get uninfected again (through recovery/removal).

   Importantly, while some quantities like $G_{\mathrm{SI}}^\infty = \infty$, $G_{\mathrm{SI}}^0 = \ln(2)$, $j_{\mathrm{SI}}^{\max} = 1/4$ obviously agree with the values one obtains for the SIR in the limit $k \to 0$, the exponential decay of j_{SI} (F3) of the logistic SI model ($k = 0$) is qualitatively different from the SIR model at times after peak time, as the SIR exponent $-\kappa(1 - k)$ tends to reach zero for $k \to 0$. In fact, the deviations between SI and the $k \to 0$ limit of the SIR get smaller with decreasing k. This can be seen by inspecting τ in the regime where it is large, and G close to G_∞. For small k one has $\kappa \simeq k$ and $\kappa(1 - k) \approx k$, as well as $G_\infty \simeq k^{-1}$ and thus, according to equation (A7),

$$\tau \simeq \tau_2 \simeq \frac{1}{k} \ln\left(\frac{1 - k\varepsilon}{1 - kG}\right) \simeq -\frac{1}{k} \ln(1 - kG) \tag{F4}$$

as k approaches zero. This relationship can be inverted to write $G \simeq k^{-1}(1 - e^{-k\tau})$. Since $e^{-k\tau} = 1 - k\tau + O(k^2)$ for any finite τ, the G approaches τ, and j thus approaches, albeit very slowly with decreasing k, the limiting $e^{-(\tau - \tau_0)}$, in agreement with the SI model (F3). To be more precise, the SIR approaches the SI in the sense

$$\lim_{k \to 0} \int_{-\infty}^{\infty} [j(\tau) - j_{\mathrm{SI}}(\tau)]^2 \, \mathrm{d}\tau = 0 \tag{F5}$$

while for any small but finite k, the SIR j still enters the regime $j \propto e^{-\kappa(1-k)\tau} \simeq e^{-k\tau}$ at some finite crossover $\tau = \tau_{\mathrm{c}} < \infty$ that can be estimated by equating this asymptotics with

equation (F3). The asymptotics of the SIR at large times is thus different from the SI, but the numerical difference between the SI and SIR results still decreases with decreasing k. To estimate τ_c in the limit of small k, one can safely use the mentioned approximations $G_\infty \simeq k^{-1}$ and $\kappa(1 - k) \simeq k$. By equating the two differential rates (69) with (73) and (F3) the governing equation for the crossover τ_c is thus $e^{-1/k}(k\varepsilon)^{-k}e^{-k\tau_c} = e^{-\tau_c}/(e^\varepsilon - 1)$, or equivalently,

$$\tau_c \simeq \frac{1}{k} + k \, \ln(k\varepsilon) - \ln(e^\varepsilon - 1) \tag{F6}$$

where we have used another relationship, $k(1 - k) \simeq k$, also valid for small k. Further assuming $k \ll \varepsilon \ll 1$, this latter expression simplifies to

$$\tau_c \simeq \frac{1}{k} - \ln(\varepsilon) \tag{F7}$$

The crossover τ_c thus increases not only strongly with decreasing k but moreover slowly with decreasing ε, and this makes equation (F5) to hold.

Another signature of qualitatively different setting between the SI and SIR at $k \to 0$ is the relationship $J_\infty = R_\infty$ for the SIR, which breaks down at $k = 0$, as R does not depend on time for $k = 0$, and thus $R_{SI}^\infty = 0$ and $I_{SI}^\infty = 1$, while the limiting behavior of the SIR model is $\lim_{k\to0} R = \lim_{k\to0} kG_\infty = 1$.

Irrespective these observations, for an arbitrary infection rate $a(t)$, the daily number of new infections as a function of time t is given for the SI model by equation (F3) with $\tau = \int_0^t a(t')dt'$.

Appendix G. Lambert's equation. Solutions and their properties

Lambert's W function [30, 31] with several applications in physics [32–37] solves the equation $z = W(z)e^{W(z)}$. It can be used to calculate the solution of transcendental equations of the form

$$e^{-cx} = a_0(x - r) \tag{G1}$$

in explicit form as

$$x = r + \frac{1}{c}W\left(\frac{ce^{-cr}}{a_0}\right) \tag{G2}$$

The two real-valued solutions are denoted by W_0 (principal) and W_{-1} (non-principal) as shown by figure 15(a). These two functions are available in scientific software such as lambertw (Matlab^R) or ProductLog (Mathematica^R).

For the purpose of this manuscript we are interested in $W(\alpha)$ and $W(\alpha_0)$ as a function of $k \in [0, 1]$, where $\alpha = -e^{-1/k}/k$ (32) and $\alpha_0 = 2\alpha/e$ (54). The two α's and their ranges are depicted as a function of k in figure 15(b). While $\alpha \in [-e^{-1}, 0]$ for any k, the $\alpha_0 \in [-2e^{-2}, 0]$. The lower bound is in each case reached at $k = 1$. One has $W_0(0) = 0$, $W_{-1}(0) = -\infty$, $W(-e^{-1}) = -1$, $W_0(-2e^{-2}) \approx -0.406$, and $W_{-1}(-2e^{-2}) = -2$ as one can verify by pluggin in these values into Lambert's equation. Accordingly, for the case of α the solutions of Lambert's equation reside in the disjunct ranges $W_0(\alpha) \in [-1, 0]$ and $W_{-1}(\alpha) \in [-\infty, -1]$. For α_0 the solutions
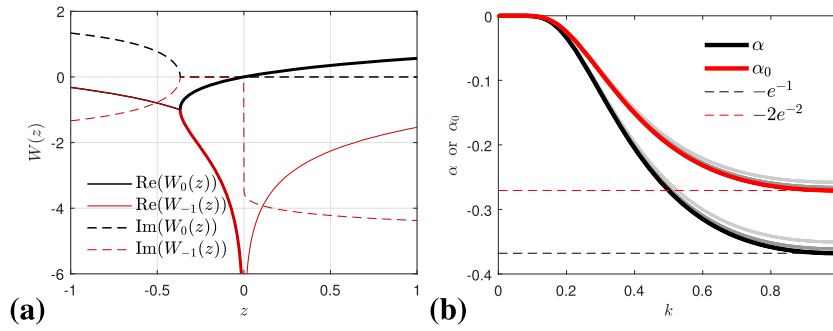
Figure 15. (a) Principal W_0 and non-principal W_{-1} solutions of Lambert's equation $z = W(z)e^{W(z)}$. As can be seen, there is single real-valued solution for $z \geqslant 0$, and two real-valued solutions for $z \in [-1/e, 0]$. Complex-valued solutions are represented by thin lines. The thick black line is the real-valued $W_0(z) \in [-1, 0]$ for $z \geqslant -1/e$, while the thick red line is the real-valued $W_{-1}(z) \leqslant -1$ for $z \in [-1/e, 0]$. (b) α and α_0 vs k for $\varepsilon = 0$ (thick), $\varepsilon = 0.02$ and $\varepsilon = 0.05$ (thin). One has $\alpha \geqslant -e^{-1} \approx -0.368$ and $\alpha_0 \geqslant -2e^{-2} \approx -0.271$ for all $k \in [0, 1]$ and $\varepsilon \geqslant 0$.

reside in the disjunct ranges $W_0(\alpha_0) \in [-0.406, 0]$ and $W_{-1}(\alpha_0) \in [-\infty, -2]$. These ranges are used to select the relevant solutions of Lambert's equation in (32) and (54). A special, trivial but important case is $z = -e^{-1/k}/k = \alpha(\varepsilon = 0)$ because this z obviously solves Lambert's equation exactly with the simple $W_{-1}(z) = -k^{-1}$, i.e., one has

$$W_{-1}\left(-\frac{e^{-1/k}}{k}\right) = -\frac{1}{k} \tag{G3}$$

for all k. Using the same α's, Lambert's W functions have the following property

$$W_0(\alpha) - W_{-1}(\alpha_0) \geqslant 1 \tag{G4}$$

that implies $G_0 \leqslant G_\infty$.

Proof. As is obvious from figure 15(b), the difference between α and α_0 is largest at $k = 1$ and $\varepsilon = 0$. For these special values $W_0(\alpha) = W_0(-e^{-1}) = -1$ and $W_{-1}(\alpha_0) = W_{-1}(2e^{-2}) = -2$. The difference then changes monotonously and becomes huge in the limit $k \to 0$ (and $\alpha \to 0$), as is obvious from figure 15(b). This completes the proof.

Another important inequality is

$$W_{-1}(\alpha) - W_{-1}(\alpha_0) \leqslant 1 \tag{G5}$$

as it implies $G_0 \geqslant G_{-\infty} = 0$.

Proof. The left-hand side increases with increasing k, as $\alpha - \alpha_0$ increases as well (figure 15(b)). At $k = 1$, $W_{-1}(\alpha) = W_{-1}(-e^{-1}) = -1$ and $W_{-1}(\alpha_0) = W_{-1}(-2e^{-2}) = -2$. This completes the proof.

There is another identity that we need to derive the final expression for our approximant $\widetilde{G}(\tau)$.

$$W(z \ \ln \ z) = \ln \ z \tag{G6}$$

holds for any $z > 0$. As a proof one can start from this expression for W, to obtain $We^W = (\ln z)e^{\ln z} = z \ln z$, which is Lambert's equation. A function W with the property (G6) fulfills Lambert's equation at the same time, as long as W is real-valued; equation (G6) is thus equivalent to Lambert's equation over the domain of positive arguments.

Taking the derivative of Lambert's equation $z = W e^W$ with respect to z, Lambert's functions W_0 and W_{-1} both obey the differential equation

$$z\frac{dW}{dz} = \frac{W(z)}{1 + W(z)} \tag{G7}$$

so that

$$x\frac{dW(cx)}{dx} = \frac{W(cx)}{1 + W(cx)}, \tag{G8}$$

$$x\frac{dW(cx)}{dx} - W(cx) = -\frac{W^2(cx)}{1 + W(cx)} \tag{G9}$$

Relationships (G8) and (G9) are required if one attempts calculating the approximant $\widetilde{j}$ from $-d\widetilde{S}/d\tau$.

For small z, Lambert's function W_0 has the expansion

$$W_0(z) = z - z^2 + \frac{3}{2}z^3 + O(z^4) \tag{G10}$$

implying

$$\frac{W_0(z)}{z} = 1 - z + \frac{3}{2}z^2 + O(z^3), \tag{G11}$$

$$\frac{W_0(z)}{1 + W_0(z)} = z - \frac{z^3}{2} + O(z^4) \tag{G12}$$

Appendix H. Cumulative $\widetilde{J}(\tau)$ for GM-like solution of the SIR

The cumulative $\widetilde{J}_{\mathrm{GML}}(\tau) = \int_{-\infty}^{\tau} \widetilde{j}_{\mathrm{GML}}(\tau')d\tau'$ corresponding to $\widetilde{j}_{\mathrm{GML}}(\tau)$ given by the GM-like equation (84) follows by integration. One has

$$\widetilde{J}_{\mathrm{GML}}(\tau) = \begin{cases} \widetilde{J}_1(\tau), & \tau \leqslant \tau_{\mathrm{early}}, \\ \widetilde{J}_1(\tau_{\mathrm{early}}) + \widetilde{J}_T(\tau), & \tau \in [\tau_{\mathrm{early}}, \tau_{\mathrm{late}}] \\ \widetilde{J}_1(\tau_{\mathrm{early}}) + \widetilde{J}_T(\tau_{\mathrm{late}}) + \widetilde{J}_2(\tau), & \tau \geqslant \tau_{\mathrm{late}} \end{cases} \tag{H1}$$
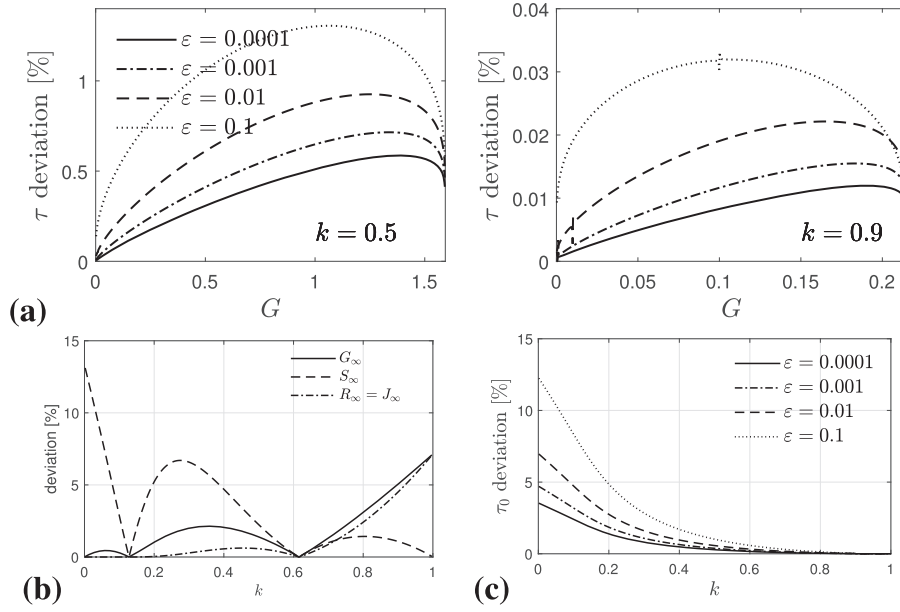
Figure 16. Absolute relative deviations between the exact and approximative analytical (a, top row) $\tau(G)$ shown in figure 1 for k = 0.5 and k = 0.9, (b) final values shown in figure 2, and (c) τ_0 shown in figure 5. Note the different scales for the panels and that the absolute error may be extremely small when the relative error is as large as 10%.

with

$$\widetilde{J}_1(\tau) = \frac{j_{\text{early}}\, e^{(1-k)(\tau-\tau_0)}}{1-k},$$

$$\widetilde{J}_T(\tau) = \frac{j_{\max}\,\omega_0\sqrt{\pi}}{2}\left[\text{erf}\left(\frac{\tau-\tau_0}{\omega_0}\right)+\text{erf}\left(\frac{\tau_0-\tau_{\text{early}}}{\omega_0}\right)\right], \tag{H2}$$

$$\widetilde{J}_2(\tau) = \frac{j_{\text{late}}\left[e^{-\kappa(1-k)(\tau_{\text{late}}-\tau_0)}-e^{-\kappa(1-k)(\tau-\tau_0)}\right]}{\kappa(1-k)}$$

Appendix I. Deviation between analytical and numerical results

Because our analytical approximants seem to reproduce the exact result so very well that it is hard to see any difference between the curves by eye, figure 16 provides some plots that show the absolute relative difference between the two.

Appendix J. Supplementary: implementation

For the convenience of a reader, this section contains a complete Mathematica™ notebook that creates time-dependent SIR results using our $\widetilde{G}(\tau)$ for an arbitrary infection rate a[t], specified in the first line, arbitrary $k \in (0, k_{\max})$ and $S(0) \in (0, 1)$. All results such as $S(t)$ (code SIRS[k,S0][t]) and $\dot{J}(t)$ (code SIRj(k,S0][t]) are available analytically, and can be plotted as shown.

```
a[t_] := 1;
tau[t_] = Integrate[a[s], {s, 0, t}];

W[type_, x_]:= ProductLog[type, x];
W0[k_]:= W[0, -Exp[-1/k]/k];
W1[k_]:= W[-1, -2 Exp[-1/k - 1]/k];
kp[k_]:= k (1 + W0[k])/(1 - k);
pk[k_]:= 1/kp[k];
f[k_][x_]:= 1 - k x - Exp[-x];
Gf[k_]:= 1/k + W0[k];
G0[k_]:= (1+k)/k + W1[k];
A[k_][x_]:=Log[(1-x/Gf[k])Power[Gf[k]/x,kp[k]]];
Ae[k_,S0_]:= A[k][-Log[S0]];
A0[k_]:= A[k][G0[k]];
jmax[k_]:=((1-k G0[k])^2-k^2)/4;
Jf[k_]:=k Gf[k];
tau0[k_,S0_]:=(Ae[k,S0]-A0[k])/(kp[k](1-k));

(* approximant G[tau] *)
g0[k_]:= G0[k]/Gf[k];
b1[k_]:= -kp[k] g0[k]/Log[1 - g0[k]];
b2[k_]:= (g0[k] - 1)/(kp[k]Log[g0[k]]);
c1[k_]:= -Log[1-g0[k]]/(kp[k]Power[1-g0[k],pk[k]]);
c2[k_]:= -kp[k]Log[g0[k]]/Power[g0[k],kp[k]];
pow1[k_]:= 1-k;
pow2[k_]:= -kp[k](1-k);
dt[k_,S0_][tau_] := tau-tau0[k,S0];
x1[k_,S0_][tau_] := Exp[pow1[k]dt[k,S0][tau]];
x2[k_,S0_][tau_] := Exp[pow2[k]dt[k,S0][tau]];
H2[k_,S0_][tau_] := HeavisideTheta[tau-tau0[k,S0]];
H1[k_,S0_][tau_] := 1-H2[k,S0][tau];
G[k_,S0_][tau_] := Gf[k](
 H1[k,S0][tau] b1[k] W[0,c1[k] x1[k, S0][tau]] +
 H2[k,S0][tau] (1-b2[k]W[0,c2[k]x2[k,S0][tau]]));

(* Analytical S,I,R,j,J as functions of time t *)
(* parameters: k and S(t=0) *)
SIRS[k_,S0_][t_]:= Exp[-G[k,S0][tau[t]]];
SIRI[k_,S0_][t_]:= f[k][G[k,S0][tau[t]]];
SIRR[k_,S0_][t_]:= k G[k,S0][tau[t]];
SIRj[k_,S0_][t_]:= SIRS[k,S0][t]SIRI[k,S0][t];
SIRJ[k_,S0_][t_]:= 1 - SIRS[k,S0][t];

(* exact numerical result for comparison (via J) *)
exactSIRtauOfJ[k_,S0_][J_]:=
 NIntegrate[1/((1-y)(y+k Log[1-y])),{y,1-S0,J}];
exactSIRSofJ[k_,S0_][J_]:=1-J;
exactSIRIofJ[k_,S0_][J_]:=(k Log[1-J]+J);
exactSIRRofJ[k_,S0_][J_]:=-k Log[1-J];
exactSIRjofJ[k_,S0_][J_]:=(k Log[1-J]+J)(1-J);

(* example *)
(* j(t) for k=0.5 and S(t=0)=0.99 *)
Plot[SIRj[0.5,0.99][t],{t,-30,30}]

ParametricPlot[{exactSIRtauOfJ[0.5,0.99][J],
 exactSIRjofJ[0.5,0.99][J]},{J,0,Jf[0.5]}
```

ORCID iDs

M Kröger ⬛ https://orcid.org/0000-0003-1402-6714

R Schlickeiser ⬛ https://orcid.org/0000-0003-3171-5079

References

[1] Li L *et al* 2020 Propagation analysis and prediction of the COVID-19 *Infect. Disease Model.* **5** 282–92

[2] Ciufolini I and Paolozzi A 2020 Mathematical prediction of the time evolution of the COVID-19 pandemic in Italy by a Gauss error function and Monte Carlo simulations *Eur. Phys. J. Plus* **135** 355

[3] Schlickeiser R and Schlickeiser F 2020 A Gaussian model for the time development of the SARS-CoV-2 corona pandemic disease. Predictions for Germany made on March 30 *Physics* **2** 164–70

[4] Schüttler J, Schlickeiser R, Schlickeiser F and Kröger M 2020 COVID-19 predictions using a Gauss model, based on data from April 2 *Physics* **2** 197–212

[5] Kermack W O and McKendrick A G 1927 A contribution to the mathematical theory of epidemics *Proc. R. Soc.* A **115** 700–21

[6] Estrada E 2020 COVID-19 and SARS-CoV-2. Modeling the present, looking at the future *Phys. Rep.* **869** 1–51

[7] Täuber U C 2014 *Critical Dynamics: A Field Theory Approach to Equilibrium and Non-Equilibrium Scaling Behavior* (Cambridge: Cambridge University Press)

[8] Lindenberg K, Metzler R and Oshanin G (ed) 2019 *Chemical Kimnetics: Beyond the Textbook* (Singapore: World Scientific)

[9] Kendall D G 1956 Deterministic and stochastic epidemics in closed populations *Proc. Third Berkeley Symp. on Mathematical Statistics and Probability* vol 4 (Berkeley: University of California Press) pp 149–65

[10] Hethcode H W 2000 The mathematics of infectious diseases *SIAM Rev.* **42** 599–653

[11] O'Regan S M, Kelly T C, Korobeinikov A, O'Callaghan M J A and Pokrovskii A V 2010 Lyapunov functions for SIR and SIRS epidemic models *Appl. Math. Lett.* **23** 446–8

[12] Satsuma J, Willox R, Ramani A, Grammaticos B and Carstea A S 2004 Extending the SIR epidemic model *Physica* A **336** 369–75

[13] Cadoni M 2020 How to reduce epidemic peaks keeping under control the time-span of the epidemic *Chaos Solitons Fractals* **138** 109940

[14] Schlickeiser R and Kröger M 2020 Epidemics forecast from SIR-modeling, verification and calculated effects of lockdown and lifting of interventions *Frontiers Phys.* (in press) https://doi.org/10.3389/fphy.2020.593421

[15] Barlow N S and Weinstein S J 2020 Accurate closed-form solution of the SIR epidemic model *Physica* D **408** 132540

[16] Barlow N S, Stanton C R, Hill N, Weinstein S J and Cio A G 2017 On the summation of divergent, truncated, and underspecified power series via asymptotic approximants *Q. J. Mech. Appl. Math.* **70** 21

[17] Cadoni M and Gaeta G 2020 Size and timescale of epidemics in the SIR framework *Physica* D **411** 132626

[18] Chekroun A and Kuniya T 2020 Global threshold dynamics of aninfection age-structured SIR epidemic model with diffusion under the Dirichlet boundary condition *J. Differ. Equ.* **269** 117–48

[19] Imron C, Hariyanto , Yunus M, Surjanto S D and Dewi N A C 2019 Stability and persistence analysis on the epidemic model multi-region multi-patches *J. Phys.: Conf. Ser.* **1218** 012035

[20] Karaji P T and Nyamoradi N 2020 Analysis of a fractional SIR model with general incidence function *Appl. Math. Lett.* **108** 106499

[21] Mohamadou Y, Halidou A and Kapen P T 2020 A review of mathematical modeling, artificial intelligence and datasets used in the study, prediction and management of COVID-19 *Appl. Intell.* **50** 3913

[22] Samanta S, Sahoo B and Das B 2019 Dynamics of an epidemic system with prey herd behavior and alternative resource to predator *J. Phys. A: Math. Theor.* **52** 425601

[23] Sene N 2020 SIR epidemic model with Mittag–Leffler fractional derivative *Chaos Solitons Fractals* **137** 109833

[24] Simon M 2020 SIR epidemics with stochastic infectious periods *Stoch. Process. Appl.* **130** 4252–74
[25] Tian C, Zhang Q and Zhang L 2020 Global stability in a networked SIR epidemic model *Appl. Math. Lett.* **107** 106444
[26] Barmparis G D and Tsironis G P 2020 Estimating the infection horizon of COVID-19 in eight countries with a data-driven approach *Chaos Solitons Fractals* **135** 109842
[27] Kolberg U and Schlickeiser R 2018 Kinetic theory of small-amplitude fluctuations in astrophysical plasmas *Phys. Rep.* **783–785** 1–84
[28] Harko T, Lobo F S N and Mak M K 2014 Exact analytical solutions of the susceptible-infected-recovered (SIR) epidemic model and of the SIR model with equal death and birth rates *Appl. Math. Comput.* **236** 184–94
[29] Kröger M and Schlickeiser R 2020 Gaussian doubling times and reproduction factors of the COVID-19 pandemic disease *Frontiers Phys.* **8** 276
[30] Lambert J H 1758 Observations variae in mathesin puram *Acta Helvetica Physico-Mathematico-Anatomico-Botanico-Medica* (Societas physico-medica, Basel, Switzerland) vol 3 pp 128–68
[31] Corless R M, Gonnet G H, Hare D E G, Jeffrey D J and Knuth D E 1996 On the Lambert W function *Adv. Comput. Math.* **5** 329–59
[32] Barry D A, Parlange J Y, Li L, Prommer H, Cunningham C J and Stagnitti E 2000 Analytical approximations for real values of the Lambert W-function *Math. Comput. Simul.* **53** 95–103
[33] Chapeau-Blondeau F and Monir A 2002 Numerical evaluation of the Lambert W function and application to generation of generalized Gaussian noise with exponent 1/2 *IEEE Trans. Signal Process.* **50** 2160–5
[34] Jain A and Kapoor A 2004 Exact analytical solutions of the parameters of real solar cells using Lambert W-function *Sol. Energy Mater. Sol. Cells* **81** 269–77
[35] Valluri S R, Jeffrey D J and Corless R M 2000 Some applications of the Lambert W function to physics *Can. J. Phys.* **78** 823–31
[36] Scott T C, Fee G, Grotendorst J and Zhang W Z 2014 Numerics of the generalized Lambert W function *ACM Commun. Comput. Algebra* **48** 42–56
[37] Scott T C, Fee G and Grotendorst J 2013 Asymptotic series of generalized Lambert W function *ACM Commun. Comput. Algebra* **47** 75–83